CERN–TH/95–62
LU TP 95–6
March 1995

Low- and high-mass components of the photon distribution functions

Gerhard A. Schuler[a]

Theory Division, CERN
CH-1211 Geneva 23, Switzerland
E-mail: schulerg@cernvm.cern.ch

and

Torbjörn Sjöstrand

Department of Theoretical Physics 2
University of Lund, Lund, Sweden
E-mail: torbjorn@thep.lu.se

Abstract

The structure of the general solution of the inhomogeneous evolution equations allows the separation of a photon structure function into perturbative ("anomalous") and non-perturbative contributions. The former part is fully calculable, and can be identified with the high-mass contributions to the dispersion integral in the photon mass. Properly normalized "state" distributions can be defined, where the $\gamma \to \mathrm{q\overline{q}}$ splitting probability is factored out. These state distributions are shown to be useful in the description of the hadronic event properties, and necessary for a proper eikonalization of jet cross sections. Convenient parametrizations are provided both for the state and for the full anomalous parton distributions. The non-perturbative parts of the parton distribution functions of the photon are identified with the low-mass contributions to the dispersion integral. Their normalizations, as well as the value of the scale Q_0 at which the perturbative parts vanish, are fixed by approximating the low-mass contributions by a discrete, finite sum of vector mesons. The shapes of these hadronic distributions are fitted to the available data on $F_2^\gamma(x, Q^2)$. Parametrizations are provided for $Q_0 = 0.6\,\mathrm{GeV}$ and $Q_0 = 2\,\mathrm{GeV}$, both in the DIS and the $\overline{\mathrm{MS}}$ factorization schemes. The full parametrizations are extended towards virtual photons. Finally, the often-used "FKP-plus-TPC/2γ" solution for $F_2^\gamma(x, Q^2)$ is commented upon.

[a] Heisenberg Fellow.

1 Introduction

Inclusive cross sections, such as deep-inelastic electron–photon scattering $e\gamma \to e + X$ or high-$p_\perp$ jet production in two-photon collisions $\gamma\gamma \to \text{jet} + X$, are fully expressed in terms of the parton distribution functions (PDFs) of the photon $f_a^\gamma(x, Q^2)$ (for recent reviews on the photon structure functions see e.g. refs. [1, 2, 3, 4, 5, 6]). Correspondingly, such measurements allow, in principle, a unique determination of the PDFs of the photon. However, already for the simplest determination, namely the extraction of $F_2^\gamma(x, Q^2)$ from deep-inelastic electron–photon scattering, additional information about the hadronic final state is necessary [7]. The reason is simple: in contrast to lepton–nucleon scattering, where (x, Q^2) are fixed by the measurement of the outgoing lepton solely, in $e\gamma$ scattering x usually can only be determined through a reconstruction of the hadronic energy W from the visible one by virtue of the relation $x = Q^2/(W^2 + Q^2)$. Clearly, an exclusive description of the event properties is not only of interest for acceptance corrections but provides also additional insight in the structure of the photon.

In this paper we shall investigate the photon-to-$q\overline{q}$ splitting probability and define (normalized) "state" distributions where this probability factor is split off. We shall show that the use of these state distributions is of great advantage in obtaining a correct description of the hadronic final state, notably of the photon remnants and the initial-state gluon radiation in parton-shower programs. We shall see that the state distributions enter also the calculation of jet cross sections at high energies where unitarity corrections have to be taken into account.

Furthermore, we shall show how to obtain a constrained parametrization of the (inclusive) PDFs of the photon. Current parametrizations either are fully unconstrained, i.e. all parameters are fitted to F_2^γ data [8], or rely on severe prejudices about the input distributions, such as approximating these by the ones of the pion [9, 10] or modelling them by the quark–parton results (box-diagram) with the quark masses as free parameters [11]. By contrast, the shapes of our input distributions are determined by the F_2^γ data, while the normalizations are constrained. There exists a one-to-one relation between the size of the non-perturbative part and the scale Q_0 introduced to separate the non-perturbative and the perturbative parts. This scale should be universal, i.e. process-independent and can, for example, be constrained by a study of the γp total cross section [12]. We also investigate the sensitivity of the PDFs to the photonic factorization scheme associated with the presence of a direct contribution C^γ to F_2^γ. The current analysis updates our old parametrization of the photon PDFs [12].

Next we discuss the dependence of the PDFs of the photon on its mass (virtuality) P^2, i.e. the so-called target-mass effects. Our parametrization can, in fact, also be used for the PDFs of a virtual photon, and we shall outline the assumptions that are behind this. Effects of a non-zero virtuality have attracted considerable interest [13, 14, 4, 15, 16, 17, 18], but no explicit (analytic) parametrization was available up to now.

The outline of the paper is as follows. In the next section we first discuss the photon-to-$q\overline{q}$ splitting and the issues of introducing a scale Q_0 to separate low-mass contributions from perturbatively calculable high-mass contributions. The latter, the so-called anomalous contributions, are then expressed in terms of "state distributions" that enter the description of the hadronic event (section 2.1), the eikonalization of jet cross sections (section 2.2), and the virtual PDFs (section 2.3). Section 3 contains details about the parametrizations of the parameter-free state distributions and the anomalous distributions. The small-x behaviour of the distribution functions is outlined. In section 4 we

discuss the normalization of the non-perturbative (low-mass) contributions to the photonic PDFs ("hadronic distributions") and compare our fits to the F_2^γ data. Finally we comment upon the often-used approximation of F_2^γ by the sum of the (Q^2-independent) TPC/2γ parametrization [19] and the QCD expression of FKP [20]. Our results are summarized in section 5. There we also discuss further aspects of our separation of the photon distribution functions into long-distance and short-distance components, in particular the connection with the representation of a photonic PDF as a dispersion integral in the photon mass.

2 Separation of the non-perturbative part

Perturbative QCD predicts only the Q^2 evolution of the PDFs of the photon $f_i^\gamma(x,Q^2)$, via a set of inhomogeneous differential equations of the first kind. Hence the solutions $f_i^\gamma(x,Q^2)$ require the specification of the PDFs at some $Q^2 = Q_0^2$. It is well known that these "input" distributions $f_i^\gamma(x,Q_0^2)$ have to have a considerable "hard" component if Q_0 is chosen to be a typical hadronic input scale ($Q_0 \gtrsim 2\,\mathrm{GeV}$). This is quite in contrast to hadronic PDFs which vanish in a powerlike way $\propto (1-x)^p$ ($p \gtrsim 1$) for $x \to 1$. Correspondingly, there is no unique guiding principle as to what the photonic input distributions should look like. Rather, parametrizations starting at large Q_0 [8, 11] are obtained by just fitting the parameters of the input distributions $f_a^\gamma(x,Q_0^2)$ (shapes and normalizations) to the available F_2^γ data. Moreover, since these data are so far restricted to large x, basically no constraint on the gluon distribution of the photon exists today in such an approach.

Lowering the starting scale Q_0 to about 0.5–0.7 GeV, it is, however, possible to describe the F_2^γ data with photonic PDFs obtained from a purely hadronic input [9, 12, 10]. The latter is usually estimated by the PDFs of the pion using vector-meson-dominance (VMD) and the additive quark model. The recent next-to-leading-order parametrizations AFG [10] and GRV [9] essentially differ in the ansatz to take the photon to be a coherent [10] or incoherent [9] superposition of vector mesons. Both are parametrizations of the inclusive PDFs of the photon. Our aim [12] is to obtain PDFs where the probability for the photon to fluctuate into a hadronic state is made explicit. Firstly, this allows us to constrain the normalizations of the non-perturbative input distributions, while the shapes are fitted to F_2^γ data. Secondly, we can trace the complete evolution of the parton showering, otherwise hidden in the expression of $f_i^\gamma(x,Q^2)$. Thirdly, differences in the remnant structure of the photon can be respected. Finally, our parametrizations hold also for a virtual photon, to which they can easily be applied because the parametrizations are analytic in both P^2 and Q^2. On the other hand, our parametrizations are leading-order ones only.

Analogously to our decomposition of the γp total cross section

$$\sigma_{\mathrm{tot}}^{\gamma\mathrm{p}} = \sigma_{\mathrm{dir}}^{\gamma\mathrm{p}} + \sigma_{\mathrm{VMD}}^{\gamma\mathrm{p}} + \sigma_{\mathrm{anom}}^{\gamma\mathrm{p}} \ , \tag{1}$$

we decompose the PDFs of the photon as

$$f_a^\gamma(x,Q^2) = f_a^{\gamma,\mathrm{dir}}(x,Q^2) + f_a^{\gamma,\mathrm{VMD}}(x,Q^2,Q_0^2) + f_a^{\gamma,\mathrm{anom}}(x,Q^2;Q_0^2) \ . \tag{2}$$

The ansatz (1), or eq. (2), is based on the assumption that there exists a scale Q_0 which divides the spectrum of $\gamma \to \mathrm{q\overline{q}}$ fluctuations: above Q_0 these can be described pertur-

batively[1] ("anomalous" term in eqs. (1) and (2)), while below Q_0 the fluctuations are assumed to give vector-meson states.

A reminder of the familiar scale ambiguity problem may be in place. In this paper we work throughout with the deep-inelastic-scattering convention in mind, where the Q^2 scale is set by the virtuality of the probing photon. Fluctuations $\gamma \leftrightarrow \mathrm{q\overline{q}}$ of the probed photon are resolved as long as the "scale" k of these fluctuations is below Q. However, the precise physics definition of k is left unspecified. When PDFs extracted from deep inelastic scattering are applied to other processes, such as $\mathrm{qq'} \to \mathrm{qq'}$ high-$p_\perp$ jet production, the choice of relevant scale Q is ambiguous. It could be associated with the transverse momentum $p_\perp$ of the jets, or some multiple thereof. Conversely, our transverse momentum cut-off, used in [12] to separate between direct, simple VMD (i.e. ρ^0, ω, and ϕ) and anomalous processes, is of the order of the $Q_0 \sim 0.6$ GeV used in this paper, but the two could well differ by some amount.

The first term in eq. (2) describes the (properly normalized) probability distribution of a photon to remain a photon

$$f_a^{\gamma,\mathrm{dir}}(x,Q^2) = Z_3\,\delta_{a\gamma}\,\delta(1-x)\ , \tag{3}$$

where

$$Z_3 = 1 - \sum_{a=\mathrm{q},\overline{\mathrm{q}},\mathrm{g}} \int_0^1 \mathrm{d}x\; x\;\left\{ f_a^{\gamma,\mathrm{VMD}}(x,Q^2,Q_0^2) + f_a^{\gamma,\mathrm{anom}}(x,Q^2;Q_0^2)\right\}\ . \tag{4}$$

Properly speaking, also fluctuations $\gamma \leftrightarrow \ell^+\ell^-$, $\ell = \mathrm{e},\mu$ or τ, should be taken into account for Z_3. This contribution is fully perturbatively calculable. In practice, $Z_3 \approx 1$ is a sufficiently good approximation for all applications.

The PDFs of the photon, being the solution of an inhomogeneous evolution equation (or, more precisely, a system of equations) can always be written as the sum of two terms

$$f_a^{\gamma}(x,Q^2) - f_a^{\gamma,\mathrm{dir}}(x,Q^2) = f_a^{\gamma,\mathrm{PT}}(x,Q^2,Q_0^2) + f_a^{\gamma,\mathrm{NP}}(x,Q^2,Q_0^2)\ . \tag{5}$$

The first term is a particular solution of the *inhomogeneous* equation with the boundary condition

$$f_a^{\gamma,\mathrm{PT}}(x,Q_0^2,Q_0^2) = 0\ . \tag{6}$$

The second term, a general solution of the corresponding *homogeneous* evolution equation needs a (non-perturbative) input distribution at $Q^2 = Q_0^2$

$$f_a^{\gamma,\mathrm{NP}}(x,Q_0^2,Q_0^2) = F_a^{\mathrm{NP}}(x)\ . \tag{7}$$

While mathematically the decomposition (5) is valid for any Q_0^2, for physics reasons we want to identify $f_a^{\gamma,\mathrm{PT}}$ with the perturbatively calculable distributions $f_a^{\gamma,\mathrm{anom}}$ arising from the point-like coupling of the photon to a quark–antiquark pair. These distributions can be expressed as an integral of "state" distribution functions $f_a^{\gamma,\mathrm{q\overline{q}}}(x,Q^2;k^2)$:

$$f_a^{\gamma,\mathrm{anom}}(x,Q^2;Q_0^2) = \frac{\alpha_{\mathrm{em}}}{2\pi}\sum_{\mathrm{q}} 2e_{\mathrm{q}}^2 \int_{Q_0^2}^{Q^2} \frac{\mathrm{d}k^2}{k^2}\, f_a^{\gamma,\mathrm{q\overline{q}}}(x,Q^2;k^2)\ , \tag{8}$$

which obey the standard, homogeneous evolution equations with the boundary condition

$$f_a^{\gamma,\mathrm{q\overline{q}}}(x,k^2;k^2) = f_a^{\gamma,\mathrm{q\overline{q}}}(x) \equiv \frac{3}{2}\left(x^2+(1-x)^2\right)\left(\delta_{a\mathrm{q}} + \delta_{a\overline{\mathrm{q}}}\right)\ . \tag{9}$$

[1] A similar definition of the perturbative part of $F_2^\gamma(x,Q^2)$ is due to FKP [20]. A comparison is postponed to section 4.5.

The solution (8) can be understood as follows. The probability for the photon to branch into a $q\overline{q}$ state at some high scale k is given by $(\alpha_{em}/2\pi)\, 2e_q^2\, dk^2/k^2$. Once the photon has fluctuated, the possibility of additional QCD evolution between k and Q is just given by the standard evolution equations. This evolution conserves total momentum, so that

$$\sum_a \int_0^1 dx\, x f_a^{\gamma,q\overline{q}}(x, Q^2; k^2) = 1 \qquad (\text{for } Q \geq k)\ , \tag{10}$$

where the sum now runs over the gluon and all the quark and antiquark species.

Similarly, $f_a^{\gamma,NP}$ should describe the partonic content of the photon that has fluctuated to a vector meson, i.e.

$$f_a^{\gamma,VMD}(x, Q^2, Q_0^2) = \sum_V \frac{4\pi\alpha_{em}}{f_V^2} f_a^{\gamma,V}(x, Q^2, Q_0^2)\ . \tag{11}$$

Here $4\pi\alpha_{em}/f_V^2$ gives the probability for the photon to fluctuate into the vector meson V, while $f_a^{\gamma,V}$ obeys a momentum sum rule just as $f_a^{\gamma,q\overline{q}}$ in eq. (10). Normally we let the sum run over ρ^0, ω and ϕ, with the first responsible for the bulk of the contribution.

In passing we note that eq. (10) yields

$$Z_3 = 1 - \sum_V \frac{4\pi\alpha_{em}}{f_V^2} - \frac{\alpha_{em}}{2\pi} \sum_q 2e_q^2 \ln\left(\frac{Q^2}{Q_0^2}\right)\ . \tag{12}$$

It is convenient to think of the anomalous component as a continuous spectrum of states, characterized by the flavour q and the scale of creation k, just as the VMD components give a discrete spectrum of states. The probability $(\alpha_{em}/2\pi)\, 2e_q^2\, dk^2/k^2$ in eq. (8) is therefore the equivalent of the VMD couplings $4\pi\alpha_{em}/f_V^2$ in eq. (11).

2.1 Hadronic event properties

For inclusive quantities, such as the high-$p_\perp$ jet rate in $\gamma\gamma$ collisions, only the full parton distributions $f_a^\gamma(x, Q^2)$ are of interest. However, for an exclusive description of event properties, states with different initial flavours and k values behave differently [21, 12]. A physically transparent description of the complete hadronic final state therefore requires that $f_a^\gamma(x, Q^2)$ be available subdivided into the $f_a^{\gamma,anom}(x, Q^2)$ and $f_a^{\gamma,VMD}(x, Q^2)$ parts, with these in their turn subdivided as an integral or sum of state distributions $f_a^{\gamma,q\overline{q}}(x, Q^2)$ and $f_a^{\gamma,V}(x, Q^2)$. Let us elaborate on this.

1. Hard processes (at a scale $p_\perp \sim Q$) in photon-induced reactions are given by the usual $2 \to 2$ partonic processes, where the parton a in the photon is selected according to the inclusive distributions $f_a^\gamma(x, Q^2)$. In addition there are the processes where the photon interacts directly, i.e. via $f_a^{\gamma,dir}(x, Q^2)$. For consistency, the direct cross sections have to be cut off at the same Q_0 as is used to define the anomalous PDFs, i.e. the cut-off will, in general, be different for different parametrizations and should be known!

2. The $2 \to 2$ partonic processes are then supplemented by initial (and final) state parton showers. In the case of partons in the photon, the inhomogeneous evolution equations have to be used. However, parametrizations of the inclusive PDFs of the photon are not guaranteed to be positive-definite at the infrared cutoff used in the parton-shower programmes. Nor is the shape at Q_0 constrained in any way to correspond to a hadronic distribution, so that it makes sense to approximate the photon remnants by those of a hadron. On the other hand, both demands are fulfilled if $f_a^\gamma(x, Q^2)$ is split as in eqs. (2),

(8) and (11). Moreover, existing parton shower programmes for homogeneous evolution, made and tested for hadron-induced reactions, can then be used, since both $f_a^{\gamma,\mathrm{q\overline{q}}}(x,Q^2;k^2)$ and $f_a^{\gamma,V}(x,Q^2)$ evolve according to the homogeneous equations. The separation (2) also ensures that the "intrinsic" transverse momentum $k_\perp$ of the initial parton in the photon can be correctly generated: a roughly Gaussian primordial $k_\perp$ distribution of width $\sim 0.5\,\mathrm{GeV}$ for low-mass hadronic fluctuations of the photon, and a $\mathrm{d}k_\perp^2/k_\perp^2$ distribution for high-mass fluctuations.

2.2 Eikonalization of jet cross-sections

The state distributions $f_a^{\gamma,\mathrm{q\overline{q}}}(x,Q^2;k^2)$ and $f_a^{\gamma,V}(x,Q^2)$ enter also the calculation of total photon-induced cross sections at high energies. There (mini)jet cross sections rise much faster than allowed by the Froissart bound and unitarization corrections have to be taken into account. Unitarization effects can be estimated by the eikonal formula. Respecting the probability for the photon to be in different hadronic fluctuations, the correct formula for e.g. γp interactions is

$$\begin{aligned}\sigma_{\mathrm{inel}}^{\gamma\mathrm{p}}(s) = \sigma_{\mathrm{dir}}^{\gamma\mathrm{p}}(s) &+ \sum_V \frac{4\pi\alpha_{\mathrm{em}}}{f_V^2} \int \mathrm{d}^2b \left\{1 - \exp\left[-2\,\mathrm{Im}\chi^{V\mathrm{p}}(s,b)\right]\right\} \\ &+ \frac{\alpha_{\mathrm{em}}}{2\pi} \sum_{\mathrm{q}} 2e_{\mathrm{q}}^2 \int_{Q_0^2} \frac{\mathrm{d}k_\perp^2}{k_\perp^2} \int \mathrm{d}^2b \left\{1 - \exp\left[-2\,\mathrm{Im}\chi^{\mathrm{q\overline{q}p}}(s,b,k_\perp^2)\right]\right\} \ . \end{aligned} \tag{13}$$

The state distributions enter the hard cross sections, e.g.

$$\sigma_{\mathrm{hard}}^{\mathrm{q\overline{q}p}}(s;k_\perp) = \int \mathrm{d}x_1 \int \mathrm{d}x_2 \int \mathrm{d}p_\perp^2 f_i^{\gamma,\mathrm{q\overline{q}}}(x_1,p_\perp^2;k_\perp) f_j^{\mathrm{p}}(x_2,p_\perp^2) \frac{\mathrm{d}\hat{\sigma}_{ij}}{\mathrm{d}p_\perp^2} \theta(p_\perp - k_\perp) \ , \tag{14}$$

which in turn enter the eikonals χ^i in eq. (13), e.g. $\chi^{\mathrm{q\overline{q}p}} = A^{\mathrm{q\overline{q}p}}\sigma^{\mathrm{q\overline{q}p}}$, where $A^{\mathrm{q\overline{q}p}}(b,k_\perp^2)$ is an overlap function and $\sigma^{\mathrm{q\overline{q}p}}(s,k_\perp^2) = \sigma_{\mathrm{soft}}^{\mathrm{q\overline{q}p}}(s,k_\perp^2) + \sigma_{\mathrm{hard}}^{\mathrm{q\overline{q}p}}(s,k_\perp^2)$.

2.3 PDFs of a virtual photon

Finally, the separation (2) is useful to study the effects of a non-zero photon virtuality P^2. Generalized vector-meson dominance suggests the following dispersion relation in k^2:

$$f_a^{\gamma^\star}(x,Q^2,P^2) = \int_0^{Q^2} \frac{\mathrm{d}k^2}{k^2} \left(\frac{k^2}{k^2+P^2}\right)^2 \frac{\alpha_{\mathrm{em}}}{2\pi} \sum_{\mathrm{q}} 2e_{\mathrm{q}}^2 f_a^{\gamma,\mathrm{q\overline{q}}}(x,Q^2;k^2) \ . \tag{15}$$

The integration from zero to Q_0^2 can be approximated by the (low-mass) vector-meson contributions, which show the usual fast P^2 fall-off predicted by pole dominance:

$$f_a^{\gamma^\star,\mathrm{VMD}}(x,Q^2,P^2) = \sum_V \left(\frac{m_V^2}{m_V^2+P^2}\right)^2 \frac{4\pi\alpha_{\mathrm{em}}}{f_V^2} f_a^{\gamma,V}(x,Q^2,P_0^2) \ . \tag{16}$$

The pole-dominance factor takes the reduced probability for a virtual photon to fluctuate into a vector meson into account. On the other hand, the PDFs of a virtual vector meson are completely unknown. The simplest choice, namely to identify them with those of a real pion, i.e. taking $P_0^2 = Q_0^2$ in eq. (16) [18], leads to unphysically large hadronic contributions at small x. Moreover, this choice does not guarantee the vanishing of the

PDFs as $P^2 \to Q^2$, as should be the case up to power-suppressed terms. Our choice $P_0^2 = \max(P^2, Q_0^2)$ is based both on this limit and on the expectation that the PDFs should become more valence-like as P^2 increases.

The anomalous contribution is given by the integration $k^2 > Q_0^2$ in eq. (15) and we approximate it by

$$f_a^{\gamma^\star,\mathrm{anom}}(x,Q^2,P^2) = \int_{\max(P^2,Q_0^2)}^{Q^2} \frac{\mathrm{d}k^2}{k^2}\,\frac{\alpha_{\mathrm{em}}}{2\pi}\,\sum_{\mathrm{q}} 2e_{\mathrm{q}}^2\, f_a^{\gamma,\mathrm{q}\overline{\mathrm{q}}}(x,Q^2;k^2)$$
$$\equiv f_a^{\gamma,\mathrm{anom}}(x,Q^2,P_0^2)\ . \tag{17}$$

The ansatz (17) guarantees that the virtual PDFs

$$f_a^{\gamma^\star}(x,Q^2,P^2) = f_a^{\gamma,\mathrm{dir}}(x,Q^2,P^2) + f_a^{\gamma^\star,\mathrm{VMD}}(x,Q^2,P^2) + f_a^{\gamma^\star,\mathrm{anom}}(x,Q^2;P^2) \tag{18}$$

are correct in the region $\Lambda^2 \ll P^2 \ll Q^2$: there the virtual PDFs can be calculated exactly and QCD predicts them to be given by eq. (8) with Q_0^2 replaced by P^2 [14]. The PDFs of eq. (18) are exact also in the limit $P^2 \to 0$ where they approach the real PDFs.

On the other hand, for P^2 of the order of Q_0^2, i.e. in the interesting "cross-over" region $P^2 \sim m_\rho^2$, the P^2 dependence of the anomalous contribution is less certain. A power-like dependence might be present that could be estimated via eq. (15). Our choice of P_0^2 in eq. (17) is motivated by (i) simplicity and (ii) the demand for a smooth transition towards higher P^2, but also alternatives like $P_0^2 = P^2 + Q_0^2$ would have fulfilled these demands. Uncertainties arising from this choice may be estimated by varying P_0^2, say, from $\max(P^2, Q_0^2/2)$ to $\max(P^2, 2Q_0^2)$.

As P^2 approaches Q^2, the concept of virtual PDFs breaks down since powerlike corrections $\propto (P^2/Q^2)^p$ then become important besides the logarithmic ones. Nevertheless, the logarithmically enhanced terms of the $P^2 \to Q^2$ limit exhibit the correct behaviour: the quark distributions approach the box-diagram expression (quark–parton model result) [13], and the gluon distribution vanishes faster than the quark ones [4]. We finally want to emphasize that our parametrization of the virtual PDFs is analytic in all variables and can hence be used easily. It is well known that hadronic distribution functions, such as $f_a^{\gamma,V}(x,Q^2,P_0^2)$, depend on the two momentum scales Q^2 and P_0^2 only through the logarithmic integration of the coupling constant (see eq. (19) below). However, also the solution of the inhomogeneous equation can be written in a similar form, see eq. (29) below.

3 The perturbative part

3.1 The state distributions

The distributions $f_a^{\gamma,\mathrm{q}\overline{\mathrm{q}}}(x,Q^2;k^2)$ depend on two momentum scales, Q and k. However, the amount of evolution that occurs between these two scales is entirely characterized by the logarithmic integration of the strong coupling constant

$$s = s(Q^2,k^2) = \int_{k^2}^{Q^2} \frac{\mathrm{d}Q^2}{Q^2}\,\frac{\alpha_{\mathrm{s}}(Q^2)}{2\pi}\ . \tag{19}$$

In leading order $s = (1/b)\,\ln[\ln(Q^2/\Lambda^2)/\ln(k^2/\Lambda^2)]$, where $b = (33-2n_f)/6$. We have here assumed that the number of flavours is fixed, e.g. $n_f = 4$, but it is straightforward to

split the Q^2 range into subranges with different n_f values and correspondingly matched $\Lambda^{(n_f)}$ values. The number of flavours also enters in the fraction of the momentum carried by gluons to that carried by quarks; here a matching between different n_f values is less transparent, but can still be attempted.

The parametrization of the quark distributions is divided into a valence and a sea part. The sea part corresponds to the distributions $f_a^{\gamma,\mathrm{q}\overline{\mathrm{q}}}$ for $a \neq \mathrm{q}, \overline{\mathrm{q}}$, while the valence part is the additional contribution obtained for $a = \mathrm{q}$ or $a = \overline{\mathrm{q}}$, i.e.

$$\begin{aligned} f_{\mathrm{q}}^{\gamma,\mathrm{q}\overline{\mathrm{q}}} &= f_{\overline{\mathrm{q}}}^{\gamma,\mathrm{q}\overline{\mathrm{q}}} = f_{\mathrm{q,val}}^{\gamma,\mathrm{q}\overline{\mathrm{q}}} + f_{\mathrm{q,sea}}^{\gamma,\mathrm{q}\overline{\mathrm{q}}} \\ f_{\mathrm{q}'}^{\gamma,\mathrm{q}\overline{\mathrm{q}}} &= f_{\overline{\mathrm{q}}'}^{\gamma,\mathrm{q}\overline{\mathrm{q}}} = f_{\mathrm{q,sea}}^{\gamma,\mathrm{q}\overline{\mathrm{q}}} \qquad \text{for } \mathrm{q}' \neq \mathrm{q} \; . \end{aligned} \tag{20}$$

As always in QCD, the solutions are too complex to be given in closed form. One therefore has to resort to approximate parametrizations. We perform an evolution in x space choosing a strategy similar to the one proposed by Odorico [22], wherein a large number of evolution histories are traced by Monte Carlo methods. The evolved parton densities are binned in x for several Q^2 values. Thereafter the x shape is parametrized in some simple form, and the Q^2 dependence of these parameters is in turn parametrized. The MINUIT program [23] is used to find suitable parametrization coefficients, but with frequent manual interaction to ensure a sensible behaviour. The fits have been made in the range $10^{-4} \leq x \leq 1$ and $Q_0 \leq Q \leq 2000 Q_0$ (where $Q_0 \approx 0.5\,\mathrm{GeV}$), but the forms have been chosen so that they can be used for all x. In regions where the distributions are large, the typical accuracy of the parametrizations is 1%–2%.

The parametrizations are

$$\begin{aligned} x f_{\mathrm{q,val}}^{\gamma,\mathrm{q}\overline{\mathrm{q}}}(x,s) &= \left(c_1^{\mathrm{val}}\, x^2 + c_2^{\mathrm{val}}\, (1-x)^2 + c_3^{\mathrm{val}}\, x(1-x) \right) x^{c_4^{\mathrm{val}}}\, (1-x^2)^{c_5^{\mathrm{val}}} \\ x f_{a,\mathrm{sea}}^{\gamma,\mathrm{q}\overline{\mathrm{q}}}(x,s) &= c_1^{\mathrm{sea}}\, x^{c_2^{\mathrm{sea}}}\, (1-x)^{c_3^{\mathrm{sea}}}\, x f_{a,\mathrm{sea,lo}}^{\gamma,\mathrm{q}\overline{\mathrm{q}}}(x) \\ x f_{\mathrm{g}}^{\gamma,\mathrm{q}\overline{\mathrm{q}}}(x,s) &= c_1^{\mathrm{g}}\, x^{c_2^{\mathrm{g}}}\, ((1-x)(-\ln x))^{c_3^{\mathrm{g}}}\, x f_{\mathrm{g,lo}}^{\gamma,\mathrm{q}\overline{\mathrm{q}}}(x) \; , \end{aligned} \tag{21}$$

where

$$x f_{a,\mathrm{sea,lo}}^{\gamma,\mathrm{q}\overline{\mathrm{q}}}(x) = \frac{8 - 73x + 62x^2}{9}(1-x) + \left(\frac{8x^2}{3} - 3 \right) x \ln x + (2x-1) x \ln^2 x \tag{22}$$

$$x f_{\mathrm{g,lo}}^{\gamma,\mathrm{q}\overline{\mathrm{q}}}(x) = \frac{4 + 7x + 4x^2}{3}(1-x) + 2x(1+x)\ln x \tag{23}$$

and the coefficients c_i are given in table 3.1.

Note that the shapes and normalizations of the parametrizations become exact in the limit $s \to 0$: the expression in eq. (9) is recovered in the limit $s \to 0$ of the valence distribution, and the gluon (sea) distribution approaches eq. (23) (eq. (22)) times $4s$ (s^2). Hence, the sea distribution vanishes faster than the gluon distribution, which in turn vanishes faster than the valence one [4]. This is because $4s f_{\mathrm{g,lo}}^{\gamma,\mathrm{q}\overline{\mathrm{q}}}(x)$ is obtained if the initial quark-distribution in eq. (9) is convoluted with the $\mathrm{q} \to \mathrm{qg}$ splitting kernel. Similarly, $s^2 f_{a,\mathrm{sea,lo}}^{\gamma,\mathrm{q}\overline{\mathrm{q}}}(x)$ is obtained if the first-order gluon-distribution in eq. (23) is convoluted with the $\mathrm{g} \to \mathrm{q}\overline{\mathrm{q}}$ splitting kernel. Moreover, our parametrizations exhibit the correct large-x behaviour, $(1-x)^{8s/3}$ for the valence distribution, $(1-x)^{1+8s/3}$ for the gluon one, and $(1-x)^{2+8s/3}$ for the sea one.

Analytic results can also be derived for the limit $x \to 0$. We find

$$x f_{\mathrm{q,val}}^{\gamma,\mathrm{q}\overline{\mathrm{q}}}(x,s) \to \frac{3}{2}\, \exp\left(\frac{2s}{3} \right)\, I_0(z_v)$$

	a	b	c	d	e	f	g
$c_1^{\rm val}$	1.5	–	–	−0.197	4.33	–	–
$c_2^{\rm val}$	1.5	2.10	–	3.29	–	–	–
$c_3^{\rm val}$	–	5.23	–	1.17	–	19.9	–
$c_4^{\rm val}$	1	–	–	1.5	–	–	–
$c_5^{\rm val}$	–	2.667	–	–	–	–	–
$c_1^{\rm sea}$	–	–	1	4.54	8.19	8.05	–
$c_2^{\rm sea}$	–	1.54	–	1.29	–	–	–
$c_3^{\rm sea}$	–	2.667	–	–	–	–	–
$c_1^{\rm g}$	–	4	–	4.76	15.2	–	29.3
$c_2^{\rm g}$	–	2.03	–	2.44	–	–	–
$c_3^{\rm g}$	–	1.333	–	–	–	–	–

Table 1: Coefficients of the state distributions parametrized in the form $c_i = (a + bs + cs^2)/(1 + ds + es^2 + fs^3 + gs^4)$.

$$xf_{\rm g}^{\gamma,{\rm q\overline{q}}}(x,s) \to \frac{8}{9}\,h(s)\sqrt{\frac{6s}{y}}\,I_1(z_g)$$
$$xf_{a,{\rm sea}}^{\gamma,{\rm q\overline{q}}}(x,s) \to \frac{8}{27}\,h(s)\,\frac{s}{y}\,I_2(z_s)\ , \tag{24}$$

where $h(s) = \exp\left[(-297 - 2n_f)s/54\right]$, $z_v = 2\sqrt{4sy/3}$, $z_s = z_g = 2\sqrt{6ys}$, and $y = \ln(1/x)$. Since $I_\nu(z) \to \exp(z)/\sqrt{2\pi z}$ for $z \to \infty$, the gluon and sea distributions grow as $\exp 2\sqrt{6s\ln(1/x)}$ at small x. However, for realistic x and Q^2 values, the distributions are far from being asymptotic, and the power-like parametrizations (21) are better suited.

The effects of quark masses have not been taken into account in the evolution. For charm (and bottom), the sea distributions should therefore be modified. Different levels of sophistication can be used. The simplest is to assume that branchings $\rm g \to c\overline{c}$ are forbidden at scales below the charm mass, while $m_{\rm c}$ can be neglected in the evolution above threshold. In this context, $m_{\rm c}$ can be thought of as an effective parameter, to be adjusted for taking into account threshold effects [24]. In the region of small s, the number of gluons increases like s, that of light sea quarks like s^2, and that of charm sea quarks like $s^2 - s_{\rm c}^2$, with $s_{\rm c} = s(\max(k^2, m_{\rm c}^2), k^2)$. For simplicity, one may thus assume

$$f_{\rm c,sea}^{\gamma,{\rm q\overline{q}}}(x,s) = \theta(s - s_{\rm c})\left(1 - \left(\frac{s_{\rm c}}{s}\right)^2\right) f_{\rm a,sea}^{\gamma,{\rm q\overline{q}}}(x,s)\ , \tag{25}$$

where $\theta(x)$ is the ordinary step function.

Also original splittings $\gamma \to {\rm c\overline{c}}$ (and $\gamma \to {\rm b\overline{b}}$) should be suppressed by mass thresholds. Again assuming a simple step threshold, one obtains $f_a^{\gamma,{\rm c\overline{c}}}(x, Q^2; k^2) = 0$ for $Q < m_{\rm c}$, while the distribution for $Q > m_{\rm c}$ is given by the substitution

$$s = s(Q^2, k^2) \to s(Q^2, \max(k^2, m_{\rm c}^2))\ . \tag{26}$$

3.2 The anomalous distributions

It would have been very convenient, had it been possible, to generate the full distributions in a simple way from the state ones above. Unfortunately, the expressions are too

complicated to allow the $\mathrm{d}k^2/k^2$ integral in eq. (8) to be carried out. The parametrization of $f_a^{\gamma,\mathrm{anom}}$ is therefore done separately from the ones given above.

The $f_a^{\gamma,\mathrm{anom}}(x,Q^2;Q_0^2)$ distributions do depend both on the Q/Λ and the Q_0/Λ ratio, and not just on a single variable. However, it is possible to separate the two dependences and to obtain a parametrization that is analytic in both Q and Q_0. Hence, our parametrization can easily be used for a virtual photon target.

To this end we introduce the functions $\overline{f}_a^{\gamma,\mathrm{q\overline{q}}}$ defined by:

$$\overline{f}_a^{\gamma,\mathrm{q\overline{q}}}(x,s_0) = \int_0^{s_0} b\,\mathrm{d}s\,\frac{\exp\left(-bs\right)}{1-\exp\left(-bs_0\right)}\,f_a^{\gamma,\mathrm{q\overline{q}}}(x,s)\ . \tag{27}$$

Here s_0 is defined analogously to s in eq. (19), i.e. $s_0 = (1/b)\,\ln[\ln(Q^2/\Lambda^2)/\ln(Q_0^2/\Lambda^2)]$. The $\overline{f}_a^{\gamma,\mathrm{q\overline{q}}}$ distributions can be seen as a weighted mean of the $f_a^{\gamma,\mathrm{q\overline{q}}}$ ones; in particular $\overline{f}_a^{\gamma,\mathrm{q\overline{q}}}$ has a unit momentum sum,

$$\sum_a \int_0^1 \mathrm{d}x\,x\overline{f}_a^{\gamma,\mathrm{q\overline{q}}}(x,s_0) = 1\ . \tag{28}$$

The information on the fraction of photons that are split by $\gamma \to \mathrm{q\overline{q}}$ is thus only carried by the prefactor proportional to $\ln(Q^2/Q_0^2)$ so that:

$$x f_a^{\gamma,\mathrm{anom}}(x,Q^2;Q_0^2) = \frac{\alpha_{\mathrm{em}}}{2\pi}\sum_{\mathrm{q}} 2e_{\mathrm{q}}^2\,\ln\left(\frac{Q^2}{Q_0^2}\right)\,x\overline{f}_a^{\gamma,\mathrm{q\overline{q}}}(x,s_0)\ . \tag{29}$$

The $\overline{f}_a^{\gamma,\mathrm{q\overline{q}}}$ have been parametrized in the same spirit as the $f_a^{\gamma,\mathrm{q\overline{q}}}$ ones, with due respect to the limiting behaviours for $s \to 0$. For the valence and sea parametrizations we take the same functional form as in eq. (21), but for the gluon we choose

$$x\overline{f}_{\mathrm{g}}^{\gamma,\mathrm{q\overline{q}}}(x,s_0) = c_1^{\mathrm{g}}\,x^{c_2^{\mathrm{g}}}\,(1-x^2)^{c_3^{\mathrm{g}}}\,x f_{\mathrm{g,lo}}^{\gamma,\mathrm{q\overline{q}}}(x)\ . \tag{30}$$

This form is not exactly like that for the gluon state-distribution, rather $((1-x)(-\ln x))^{c_3}$ is replaced by $(1-x^2)^{c_3}$. We have attempted to use the same form in both cases, but then failed to obtain reasonable fits. The limit $s \to 0$ is again exact. The coefficients c_i are collected in table 2.

The small-x behaviour is again better described by a powerlike distribution over the relevant x ranges, even though asymptotically the growth is weaker, for example

$$x\ f_{\mathrm{g}}^{\gamma,\mathrm{anom}}(x,Q^2,Q_0^2) \overset{x\to 0}{\to} \frac{\alpha_{\mathrm{em}}}{2\pi}\ \left(\sum_f 2e_f^2\right)\ \ln\frac{Q^2}{\Lambda^2}\ \frac{8bs}{9y}\ \exp\left(-\frac{297-8n_f}{27}\,s\right)\ I_2(z_g)\ . \tag{31}$$

The charm (and bottom) seas are suppressed; close to threshold by a relative amount $1-(s_{\mathrm{c}}/s)^3$, where $s_{\mathrm{c}} = s(\max(Q_0^2,m_{\mathrm{c}}^2),Q_0^2)$. (Note that this factor approaches unity faster than the factor in eq. (25), as a consequence of having a spectrum of initial branchings at different k^2 scales.) For $Q > m_{\mathrm{c}}$, the charm sea is therefore assumed to be given by the normal sea multiplied by this factor.

From the above formulae, the full distribution is built up by summing the contributions from the allowed flavours as already specified in eq. (29). Branchings $\gamma \to \mathrm{c\overline{c}}$ (and $\gamma \to \mathrm{b\overline{b}}$) do not contribute below threshold. Above threshold, the charm contribution is obtained by substituting $\max(Q_0^2,m_{\mathrm{c}}^2)$ for Q_0^2 in the logarithmic prefactor and in the definition of s.

	a	b	c	d	e	f	g
$c_1^{\rm val}$	1.5	2.49	26.9	–	32.3	–	–
$c_2^{\rm val}$	1.5	−0.49	7.83	–	7.68	–	–
$c_3^{\rm val}$	–	1.5	–	−3.2	7.	–	–
$c_4^{\rm val}$	1	–	–	0.58	–	–	–
$c_5^{\rm val}$	–	2.5	–	10.	–	–	–
$c_1^{\rm sea}$	–	–	0.333	4.90	4.69	21.4	–
$c_2^{\rm sea}$	–	−1.18	–	1.22	–	–	–
$c_3^{\rm sea}$	–	1.22	–	–	–	–	–
$c_1^{\rm g}$	–	2	–	4.	7.	–	–
$c_2^{\rm g}$	–	−1.67	–	2.	–	–	–
$c_3^{\rm g}$	–	1.2	–	–	–	–	–

Table 2: Coefficients of the full distributions parametrized as in table 3.1.

3.3 The heavy-flavour contribution

The above treatment of heavy-flavour branchings $\gamma \to c\overline{c}, b\overline{b}$ is not unreasonable for jet production in $\gamma\gamma$ collisions of real photons, $Q^2 = P^2 = 0$ (with the rôle of hard scale here taken by the transverse mass of the quarks). However, in the deep-inelastic-scattering region, $Q^2 \gg P^2 \approx 0$, the kinematics constraint $W^2 = Q^2(1-x)/x > 4m_c^2$ implies that the distribution can only be non-vanishing for $x < Q^2/(Q^2 + 4m_c^2)$. The large charm-quark charge ensures that the charm contribution is very significant for the shape of the $F_2^\gamma(x, Q^2)$ distribution.

For the charm contribution to F_2^γ, we have therefore based ourselves on the leading-order "Bethe–Heitler" cross section for $\gamma^*\gamma^* \to c\overline{c}$. (An additional charm contribution comes from our sea parametrization, i.e. from $g \to c\overline{c}$ branchings.) The full expression is given in [25], but for our applications it is sufficient to use the approximation in [26], valid in the limit $4x^2P^2 \ll Q^2$:

$$\begin{aligned} xc(x,Q^2) = \frac{\alpha_{\rm em}}{2\pi} 3 \left(\frac{2}{3}\right)^2 x \, \Bigg\{ & \beta_c \left[6x(1-x) - 1\right] \\ & + \log\left(\frac{1+\beta_c\eta_c}{1-\beta_c\eta_c}\right) \left[x^2 + (1-x)^2 + r_c x(1-3x) - \frac{1}{2} r_c^2 x^2\right] \\ & + \frac{2x}{Q^2} \frac{2\beta_c\eta_c}{1-\beta_c^2\eta_c^2} \left[(2-r_c)m_c^2 x - P^2 x\right] \Bigg\} \ , \end{aligned} \tag{32}$$

with

$$r_c = \frac{4m_c^2}{Q^2} \ , \qquad \beta_c = \sqrt{1 - \frac{4m_c^2}{W^2}} \ , \qquad \eta_c = \sqrt{1 - \frac{4x^2P^2}{Q^2}} \ , \tag{33}$$

and correspondingly for b.

Some distance above the threshold, the Bethe–Heither formula gives essentially the same contribution to F_2^γ as does the standard formulae presented in the previous section.

In the calculations, we have used fairly small c and b masses, $m_c = 1.3$ GeV and $m_b = 4.6$ GeV, so that the charm contribution is large. On the other hand, the J/ψ and Υ states are not included in the VMD sum over vector mesons. To first approximation, these two effects should therefore cancel. The approach can be motivated by standard duality arguments.

4 The non-perturbative part

4.1 Normalization

We now turn to the hadronic input distributions $f_a^{\gamma,V}(x) = f_a^{\gamma,V}(x, Q_0^2, Q_0^2)$, cf. eq. (11). Usually these are estimated by the pion PDFs using VMD and the additive quark model. Of course, the PDFs of the $q\overline{q}$ "bound states" of the photon need not be the same as those of real vector mesons. Moreover, the PDFs of the short-lived ρ^0-meson may well differ in shape from those of the long-lived pion. Therefore, in contrast to the GRV [9] and AFG [10] parametrizations, we do not approximate the hadronic input distributions $f_a^{\gamma,V}(x)$ by the pion input distributions $f_a^{\pi}(x)$, but rather constrain the shape of the input distributions from data.

We do, however, use VMD to fix the normalization of the input distributions. Indeed, for consistency with eq. (1) we cannot allow for an extra "K-factor" as is introduced in refs. [9, 10] if the input scale Q_0 corresponds to the simple ρ^0, ω, ϕ VMD model. Based on eqs. (5), (8) and (11) one has

$$\begin{aligned} &f_a^{\gamma}(x,Q^2) - f_a^{\gamma,\mathrm{dir}}(x,Q^2) = \\ &\sum_V \frac{4\pi\alpha_{\mathrm{em}}}{f_V^2} f_a^{\gamma,V}(x,Q^2,Q_0^2) + \frac{\alpha_{\mathrm{em}}}{2\pi} \sum_{\mathrm{q}} 2e_{\mathrm{q}}^2 \int_{Q_0^2}^{Q^2} \frac{\mathrm{d}k^2}{k^2}\, f_a^{\gamma,\mathrm{q}\overline{\mathrm{q}}}(x,Q^2;k^2) \;. \end{aligned} \tag{34}$$

The analogous decomposition (1) of the γp total cross section tells us that Q_0 should be of the order of 600 MeV if the sum over vector mesons includes only the three lowest-lying states $V_1 = \rho^0$, ω, and ϕ. On the other hand, for larger values of Q_0 more vector mesons V_n have to be included:

$$\sum_{V=\rho^0,\omega,\phi} \frac{e}{f_V}|V\rangle \Longrightarrow \sum_{n=1}^{N(Q_0)} \sum_{V=\rho^0,\omega,\phi} \frac{e}{f_{V_n}}|V_n\rangle \;. \tag{35}$$

Since the VMD couplings of such higher-mass states are poorly known, mass effects become more important. Moreover, the input distributions will anyhow be fitted, so we may approximate

$$\sum_{n=1}^{N(Q_0)} \sum_{V=\rho^0,\omega,\phi} \frac{4\pi\alpha_{\mathrm{em}}}{f_{V_n}^2} f_a^{\gamma,V_n}(x) \approx K \sum_{V=\rho^0,\omega,\phi} \frac{4\pi\alpha_{\mathrm{em}}}{f_V^2} \tilde{f}_a^{\gamma,V}(x) \;. \tag{36}$$

In principle, for a given Q_0, $K = K(Q_0)$ could be determined by repeating the γp total cross-section analysis. In the following we will consider two cases, (i) $Q_0 = 0.6\,\mathrm{GeV}$ and $K = 1$ fixed from the γp analysis, and (ii) $Q_0 = 2\,\mathrm{GeV}$, where K will be fitted together with the input distributions $\tilde{f}(x)$ to the $F_2^{\gamma}(x,Q^2)$ data.

The normalization of the PDFs discussed so far still leaves us freedom of how to add the vector mesons. For example, in the case of simple VMD:

$$|\gamma\rangle_{\mathrm{VMD}} = \sum_{V=\rho,\omega,\phi} \frac{e}{f_V}\,|V\rangle = \sqrt{\frac{e^2}{f_\rho^2} + \frac{e^2}{f_\omega^2}}\;\left(e_{\mathrm{u}}^2 + e_{\mathrm{d}}^2\right)^{-1/2}\;\left(e_{\mathrm{u}}\,|\mathrm{u}\overline{\mathrm{u}}\rangle + e_{\mathrm{d}}\,|\mathrm{d}\overline{\mathrm{d}}\rangle\right) + \frac{e}{f_\phi}\,|\mathrm{s}\overline{\mathrm{s}}\rangle \;. \tag{37}$$

The coherent superposition of vector mesons is obtained for $e_{\mathrm{u}} = 2/3$, $e_{\mathrm{d}} = -1/3$. A completely SU_3-symmetric coherent superposition would give $f_\rho/f_\omega = 1/3$ and

a	Incoherent		Coherent		Coherent (naive SU_3)	
u-val	$(g_\rho^2+g_\omega^2)/2$	≈ 0.248	$4(g_\rho^2+g_\omega^2)/5$	≈ 0.397	$8g_\rho^2/9$	≈ 0.404
u-sea	$g_\rho^2+g_\omega^2+g_\phi^2$	≈ 0.551	$g_\rho^2+g_\omega^2+g_\phi^2$	≈ 0.551	$4g_\rho^2/3$	≈ 0.606
d-val	$(g_\rho^2+g_\omega^2)/2$	≈ 0.248	$(g_\rho^2+g_\omega^2)/5$	≈ 0.099	$2g_\rho^2/9$	≈ 0.101
d-sea	$g_\rho^2+g_\omega^2+g_\phi^2$	≈ 0.551	$g_\rho^2+g_\omega^2+g_\phi^2$	≈ 0.551	$4g_\rho^2/3$	≈ 0.606
s-val	g_ϕ^2	≈ 0.054	g_ϕ^2	≈ 0.054	$2g_\rho^2/9$	≈ 0.101
s-sea	$g_\rho^2+g_\omega^2+g_\phi^2$	≈ 0.551	$g_\rho^2+g_\omega^2+g_\phi^2$	≈ 0.551	$4g_\rho^2/3$	≈ 0.606
gluon	$g_\rho^2+g_\omega^2+g_\phi^2$	≈ 0.551	$g_\rho^2+g_\omega^2+g_\phi^2$	≈ 0.551	$4g_\rho^2/3$	≈ 0.606

Table 3: The coefficients c_a of (38) for coherent and incoherent superpositions of vector mesons. Here $g_V^2 = 4\pi/f_V^2$.

$f_\rho/f_\phi = -\sqrt{2}/3$. This is close to the experimental numbers, but in particular ϕ production seems suppressed compared to the above expectation. This is not unreasonable in view of the larger s quark and ϕ meson masses. We therefore keep the VMD couplings at their measured values, which we also use for the total cross section in eq. (1). An incoherent superposition of u and d quarks corresponds to $e_\mathrm{u} = e_\mathrm{d} = 1$. At long time scales, e.g. in "elastic" processes such as $\gamma\mathrm{p} \to V\mathrm{p}$, the ρ^0 and ω vector mesons contain equal amounts of $\mathrm{u}\overline{\mathrm{u}}$ and $\mathrm{d}\overline{\mathrm{d}}$, i.e. the coherence at the $\gamma\mathrm{q}\overline{\mathrm{q}}$ vertex is broken. It is therefore conceivable to have either physics scenario, or some intermediate thereof, and both have been used in the literature [1, 9, 10]. Here we favour the coherent superposition of u and d quarks, in line with the argument that hard processes probe short time scales.

For the input distributions we assume an SU_3-symmetric sea distribution $s(x)$ and denote by $v(x)$ the input valence distribution such that $\Sigma \equiv \sum_\mathrm{q}(xq(x) + x\bar{q}(x)) = 2v(x) + 6s(x)$. The coefficients of the various hadronic input distributions $f_a^{\gamma,\mathrm{VMD}}(x)$ are summarized in table 3 for the three possibilities of photon decomposition discussed above, and for $K = 1$. We have used an obvious notation, e.g.

$$f_{a,\mathrm{val}}^{\gamma,\mathrm{VMD}}(x, Q_0^2, Q_0^2) = \alpha_\mathrm{em}\, c_{a,\mathrm{val}}\, v(x) \;, \tag{38}$$

and our preferred choice corresponds to the middle column in table 3. For completeness, we list also the expression of F_2 in terms of $s(x)$ and $v(x)$ for this choice

$$\begin{aligned}\frac{1}{\alpha_\mathrm{em}}\, F_2^{\gamma,\mathrm{VMD}}(x,Q^2) &= \left[\frac{34}{45}\left(\frac{4\pi}{f_\rho^2}+\frac{4\pi}{f_\omega^2}\right)+\frac{2}{9}\frac{4\pi}{f_\phi^2}\right]\, x\; v(x) + \frac{4}{3}\sum_{V=\rho,\omega,\phi}\frac{4\pi}{f_V^2}\, x\; s(x) \\ &= 0.3875\, x\; v(x) + 0.735\, x\; s(x)\;. \end{aligned} \tag{39}$$

We choose the following ansatz for the input valence distribution

$$x\, v(x) = N_v\, x^{a_v}(1-x)^{b_v}\left[1 + C_v\sqrt{x}\right] \tag{40}$$

and analogous forms for the sea and gluon distributions. Note that, since we fix the normalization of the hadronic input distributions using VMD, we can exploit two constraints, namely the number of valence quarks and the momentum sum rule

$$\int_0^1 \mathrm{d}x\, 2v(x) = 2 \quad ; \quad \int_0^1 \mathrm{d}x \sum_a x\; f_a(x) = 1\;. \tag{41}$$

4.2 Direct contribution

In contrast to the proton structure function F_2^p, the photon structure function F_2^γ receives a direct contribution beyond LO accuracy, symbolically

$$F_2^\gamma(x,Q^2) = \sum_{\rm q} e_{\rm q}^2 \left[f_{\rm q}^\gamma + f_{\overline{\rm q}}^\gamma \right] \otimes C_{\rm q} + f_{\rm g}^\gamma \otimes C_{\rm g} + C^\gamma \ . \tag{42}$$

(Note that summation over q does not automatically include antiquarks as well; the additional $\overline{\rm q}$ contribution is reflected in a factor 2 in many of the subsequent formulae.) In fact, at the relatively large x values currently probed, the inclusion of the direct term

$$C^\gamma(x) = 2\ \frac{\alpha_{\rm em}}{2\pi}\, 3 \sum_{\rm q} e_{\rm q}^4\ x\ \left\{ \left[x^2 + (1-x)^2 \right] \ln \frac{1-x}{x} + 8x(1-x) - 1 \right\} \tag{43}$$

is much more important than the modification in the Q^2 evolution when going from LO to NLO. Inclusion of C^γ defines the $\overline{\rm MS}$ scheme, while $C^\gamma = 0$ defines the DIS scheme. At any order in perturbation theory, the theoretical prediction for F_2 is scheme-dependent. This factorization-scheme dependence is reduced when including higher-order contributions (i.e. when going from LO to NLO to NNLO etc.). Many cross sections in γp and $\gamma\gamma$ are still calculated in LO accuracy. In order to investigate the factorization-scheme dependence associated with a LO calculation we shall fit PDFs in LO for both schemes

$$\begin{aligned} {\rm DIS}:\ & F_2^\gamma(x,Q^2) = 2 \sum_{\rm q} e_{\rm q}^2 f_{\rm q}^\gamma(x,Q^2) \\ \overline{\rm MS}:\ & F_2^\gamma(x,Q^2) = 2 \sum_{\rm q} e_{\rm q}^2 f_{\rm q}^\gamma(x,Q^2) + C^\gamma(x) \ , \end{aligned} \tag{44}$$

although formally C^γ is of NLO. However, we only take that part of C^γ that is universal [10], namely

$$C^\gamma(x) = 2\ \frac{\alpha_{\rm em}}{2\pi}\, 3 \sum_{\rm q} e_{\rm q}^4\ x\ \left\{ \left[x^2 + (1-x)^2 \right] \ln \frac{1}{x} + 6x(1-x) - 1 \right\} \ . \tag{45}$$

This modified expression follows from a careful analysis of the ladder diagrams, but can also be obtained by simply imposing a t (and u) cut t_0 on the box diagram to separate the perturbative (point-like) from the non-perturbative (hadronic) parts resulting in

$$\begin{aligned} & F_2^{\gamma,{\rm box}}(x,Q^2) = \\ & 2\ \frac{\alpha_{\rm em}}{2\pi}\, 3 \sum_{\rm q} e_{\rm q}^4\ x\ \left\{ \left[x^2 + (1-x)^2 \right] \ln \frac{t_{\rm max} - t_0}{t_0} + \left[6x(1-x) - 1 \right] \left(1 - \frac{2t_0}{t_{\rm max}} \right) \right\} \end{aligned} \tag{46}$$

with $t_{\rm max} = Q^2/x$. Upon dropping the higher-twist terms ($\propto 1/Q^2$), eq. (46) yields eq. (45). There is no point in keeping the higher-twist contribution in C^γ when neglecting the further (unknown) higher-twist contributions to F_2^γ. Since charm (and bottom) are included by the Bethe-Heitler formulae, they are not affected by the considerations in this section. Hence the quark sum here only runs over u, d and s quarks.

4.3 Low-Q_0 fit

The F_2^γ data are not yet precise enough for the QCD scale parameter Λ to be fitted. Therefore we fix (one-loop) $\Lambda(n_f = 3) = 230\,\mathrm{MeV}$ corresponding to $\Lambda(n_f = 4) = 200\,\mathrm{MeV}$. Moreover, for $K = 1$, $Q_0 = 0.6\,\mathrm{GeV}$ is fixed from our γp analysis. In the DIS scheme, the simplest choice, a valence-like input ($N_s = 0$ and $g(x) \propto v(x)$ with $v(x = 0) = 0$), results in a reasonable χ^2 only for a considerably smaller $Q_0 \sim 0.4\,\mathrm{GeV}$. Therefore we allow for sea-like input distributions. As the data do not require non-zero values for the parameters a_s and C_i, cf. eq. (40), we simply put these parameters equal to zero. The b_g and b_s are poorly constrained, and have therefore been assumed to be given by $b_g = b_v + 1$, $b_s = b_v + 3$. Finally, $a_g = a_v/2$ is not inconsistent with the data and has been fixed. Then we find in the DIS scheme

$$\begin{aligned} &\text{set SaS 1D} \quad \text{input :} \\ &\qquad \text{DIS :} \qquad Q_0 = 0.6\,\mathrm{GeV} \quad , \quad \Lambda = 0.2\,\mathrm{GeV} \\ &\qquad x\ v(x) = 1.294 x^{0.80}(1-x)^{0.76} \\ &\qquad x\ s(x) = 0.100(1-x)^{3.76} \\ &\qquad x\ g(x) = 1.273 x^{0.40}(1-x)^{1.76} \end{aligned} \tag{47}$$

at a χ^2 of 141 for 71 F_2^γ data points. Note that we have included also the low-Q^2 points ($Q^2 = 0.71\,\mathrm{GeV}^2$) in the fit. At the input scale $Q = Q_0$, the photon momentum is split according to about 5 : 1 : 2 between the (two) valence quarks, the (six) sea quarks, and the gluon.

In the $\overline{\mathrm{MS}}$ scheme the fit favours a small sea and we find

$$\begin{aligned} &\text{set SaS 1M} \quad \text{input :} \\ &\qquad \overline{\mathrm{MS}}\text{ :} \qquad Q_0 = 0.6\,\mathrm{GeV} \quad , \quad \Lambda = 0.2\,\mathrm{GeV} \\ &\qquad x\ v(x) = 0.8477 x^{0.51}(1-x)^{1.37} \\ &\qquad x\ s(x) = 0 \\ &\qquad x\ g(x) = 3.42 x^{0.255}(1-x)^{2.37} \end{aligned} \tag{48}$$

at a χ^2 of 136, where the photon momentum is now split according to about 7 : 0 : 13 at the input scale $Q = Q_0$. Both Q^2-evolved PDFs are parametrized as

$$x f_a^{\gamma,\mathrm{VMD}}(x,s) = c_1^a\, x^{c_2^a}\,(1-x)^{c_3^a}\,[-\ln x]^{c_4^a} + c_5^a\, x^{c_6^a}\,(1-x)^{c_7^a} \quad a = \mathrm{q,val},\ \mathrm{q,sea},\ \mathrm{g}\ , \tag{49}$$

and the coefficients c_i are given in tables 4 and 5, respectively. The coefficients c_5–c_7 are only listed in those cases where the second term was included.

Figure 1 shows $F_2^\gamma(x, Q^2)$ data compared with the predictions of our sets. As explained above, these consist of a VMD part (different for the two sets), an anomalous part for u, d and s quarks (in common), Bethe–Heitler terms for c and b production (also in common), and, for set 1M only, the C^γ term for u, d and s quarks. This subdivision is illustrated in Fig. 2, for one specific Q^2 scale. With the rather low value of Q_0, the anomalous contribution quickly becomes the dominant one. At higher Q^2 and smaller x, also the charm contribution is important. In the $\overline{\mathrm{MS}}$ scheme the hadronic distributions vanish faster with x than in the DIS scheme, both since the C^γ term is negative at large x and since the $(1-x)$-power is larger.

A reasonable description is obtained for all Q^2, although there might be a slight incompatibility between the low- and high-Q^2 data, which is also reflected in the not quite

	a	b	c	d	e	f	g	κ
$c_1^{\rm val}$	1.294	–	–	–	0.252	3.079	–	–
$c_2^{\rm val}$	0.80	−0.13	–	–	–	–	–	–
$c_3^{\rm val}$	0.76	0.667	–	–	–	–	–	–
$c_4^{\rm val}$	–	2.0	–	–	–	–	–	–
$c_1^{\rm sea}$	0.1	–	−0.397	1.121	–	5.61	5.26	–
$c_2^{\rm sea}$	–	–	−7.32	–	–	10.3	–	–
$c_3^{\rm sea}$	3.76	15.0	12.0	–	4.0	–	–	–
$c_4^{\rm sea}$	–	–	–	–	–	–	–	–
$c_1^{\rm g}$	–	7.90	–	–	5.50	–	–	5.16
$c_2^{\rm g}$	–	−1.9	–	–	3.6	–	–	–
$c_3^{\rm g}$	1.3	–	–	–	–	–	–	–
$c_4^{\rm g}$	0.5	3.0	–	–	–	–	–	–
$c_5^{\rm g}$	1.273	–	–	–	–	–	–	10.0
$c_6^{\rm g}$	0.4	–	–	–	–	–	–	–
$c_7^{\rm g}$	1.76	3.0	–	–	–	–	–	–

Table 4: Coefficients of the hadronic distributions evolved from (47), parametrized in the form (49), where $c_i = \exp(-\kappa s)(a + bs + cs^2 + ds^3)/(1 + es + fs^2 + gs^3)$.

	a	b	c	d	e	f	g	κ
$c_1^{\rm val}$	0.8477	–	–	–	1.37	2.18	3.73	–
$c_2^{\rm val}$	0.51	0.21	–	–	–	–	–	–
$c_3^{\rm val}$	1.37	–	–	–	–	–	–	–
$c_4^{\rm val}$	–	2.667	–	–	–	–	–	–
$c_1^{\rm sea}$	–	0.842	–	–	21.3	−33.2	229.	–
$c_2^{\rm sea}$	0.13	−2.90	–	–	5.44	–	–	–
$c_3^{\rm sea}$	3.45	0.5	–	–	–	–	–	–
$c_4^{\rm sea}$	2.8	–	–	–	–	–	–	–
$c_1^{\rm g}$	–	24.0	–	–	9.6	0.92	14.34	5.94
$c_2^{\rm g}$	−0.013	−1.8	–	–	3.14	–	–	–
$c_3^{\rm g}$	2.37	0.4	–	–	–	–	–	–
$c_4^{\rm g}$	0.32	3.6	–	–	–	–	–	–
$c_5^{\rm g}$	3.42	–	–	–	–	–	–	12.0
$c_6^{\rm g}$	0.255	–	–	–	–	–	–	–
$c_7^{\rm g}$	2.37	3.0	–	–	–	–	–	–

Table 5: Coefficients of the hadronic distributions evolved from (48), parametrized in the form (49), where $c_i = \exp(-\kappa s)(a + bs + cs^2 + ds^3)/(1 + es + fs^2 + gs^3)$.

optimal χ^2. This could indicate that higher-twist contributions are not negligible at low Q^2. One can imagine a situation in which higher-twist contributions significantly affect F_2, but where the leading-twist evolution of PDFs is still valid down to $Q_0 = 0.6\,\mathrm{GeV}$. In fact, including only the $F_2^\gamma(x, Q^2)$ data above $Q^2 = 4\,\mathrm{GeV}^2$ improves the fit to a χ^2 of 60 (78) in the $\overline{\mathrm{MS}}$ (DIS) scheme at now 55 data points. However, in both cases a very large sea component is needed. Therefore we do not provide such a parametrization but rather one where we also take a large $Q_0 = 2\,\mathrm{GeV}$.

The distributions (47) vanish as $x \to 1$, as do truly hadronic distributions. In order to check whether the data prefer a harder (point-like) component we added a term $N_v d_v x$ to eq. (40) but found no improvement in χ^2. We checked also the normalization of the VMD couplings by allowing the values g_i^2 in table 3 to be multiplied by an overall constant K. Interestingly enough, the data do not really require values for the VMD couplings that deviate notably from their values used in the description of γp cross sections. The fit gives $K = 1.17$ with only a slightly better χ^2 (136 compared to 141). This 17% deviation of K from unity is within the range of uncertainty of the g_i^2. For example, using $f_\rho^2/4\pi = 2.02$, as extracted from the leptonic width alone, gives a 9% increase compared to the value we use, namely 2.20, which is the geometrical mean between this "leptonic" value and the value extracted from $\gamma\mathrm{p} \to \rho^0\mathrm{p}$.

4.4 High-Q_0 fit

Alternatively we fit input distributions starting at a "typical" deep-inelastic Q_0 value, namely $Q_0 = 2\,\mathrm{GeV}$. Fixing again Λ_4 at 200 MeV, as well as $a_s = a_g = C_i = 0$, $b_s = 4$, $b_g = 2$, we find in the DIS scheme $K = 2.422$ (corresponding to additionally allowed vector mesons between 0.6 GeV and 2 GeV) and

$$\begin{aligned}
&\text{set SaS 2D} \quad \text{input :} \\
&\qquad \text{DIS :} \qquad Q_0 = 2\,\mathrm{GeV} \quad , \quad \Lambda = 0.2\,\mathrm{GeV} \quad , \quad K = 2.422 \\
&Kx\ v(x) = 1.00\left[x^{0.46}(1-x)^{0.64} + 0.76x\right] \\
&Kx\ s(x) = 0.242(1-x)^4 \\
&Kx\ g(x) = 1.925(1-x)^2
\end{aligned} \tag{50}$$

with $\chi^2 = 59$ for 55 F_2^γ data points above $Q^2 = 4\,\mathrm{GeV}^2$. In this case the photon momentum is split as about 5 : 1 : 2 between valence quarks, sea quarks, and gluons, where the "hadronic" term and the "hard" term in eq. (50) contribute each about 50% to the valence momentum. As can be seen from Fig. 1, this fit describes the high-Q^2 data better than the fit starting at $Q_0 = 0.6\,\mathrm{GeV}$, however, at the expense of not accommodating the low-Q^2 data.

As in the case of the low-Q^2 fits, the fit in the $\overline{\mathrm{MS}}$ scheme again favours softer distribution functions and we find

$$\begin{aligned}
&\text{set SaS 2M} \quad \text{input :} \\
&\qquad \overline{\mathrm{MS}}\text{ :} \qquad Q_0 = 2\,\mathrm{GeV} \quad , \quad \Lambda = 0.2\,\mathrm{GeV} \quad , \quad K = 2.094 \\
&Kx\ v(x) = 1.168\left[x^{0.50}(1-x)^{2.60} + 0.826x\right] \\
&Kx\ s(x) = 0.209(1-x)^4 \\
&Kx\ g(x) = 1.808(1-x)^2
\end{aligned} \tag{51}$$

	a	b	c	d	e	f	g	κ
$c_1^{\rm val}$	1.0	0.186	–	–	−0.209	1.495	–	–
$c_2^{\rm val}$	0.46	0.25	–	–	–	–	–	–
$c_3^{\rm val}$	0.64	0.14	5.0	–	1.0	–	–	–
$c_4^{\rm val}$	–	1.9	–	–	–	–	–	–
$c_5^{\rm val}$	0.76	0.4	–	–	–	–	–	–
$c_6^{\rm val}$	1.0	–	–	–	–	–	–	–
$c_7^{\rm val}$	–	2.667	–	–	–	–	–	–
$c_1^{\rm sea}$	0.242	−0.252	1.19	–	−0.607	21.95	–	–
$c_2^{\rm sea}$	–	–	−12.1	–	2.62	16.7	–	–
$c_3^{\rm sea}$	4.0	–	–	–	–	–	–	–
$c_4^{\rm sea}$	–	1.0	–	–	–	–	–	–
$c_1^{\rm g}$	1.925	5.55	147.	–	−3.59	3.32	–	18.67
$c_2^{\rm g}$	–	−5.81	−5.34	–	29.0	−4.26	–	–
$c_3^{\rm g}$	2.0	−5.9	–	–	1.7	–	–	–
$c_4^{\rm g}$	–	9.3	–	–	1.7	–	–	–

Table 6: Coefficients of the hadronic distributions evolved from (50), parametrized in the form (49), where $c_i = \exp(-\kappa s)(a + bs + cs^2 + ds^3)/(1 + es + fs^2 + gs^3)$.

with the same χ^2 and a slightly larger gluon-momentum fraction (29% compared to 27%). The comparison with data and the low-Q^2 fit is given in Fig. 1.

The breakdown of the two sets component by component is again shown in Fig. 2. Owing to the larger Q_0 scale, the anomalous component is small at the lower Q^2 range. Note that the Bethe–Heitler contribution to $c\overline{c}$ production remains unchanged, since we do not include an increased amount (or, indeed, any amount at all) of J/ψ production in the VMD component and therefore are allowed to maintain the same $m_c = 1.3$ GeV as was used for the low-Q_0 fits.

The distributions have again been parametrized according to eq. (49), with coefficients given in tables 6 and 7, respectively.

The current uncertainties in the PDFs of the photon are displayed in Fig. 3, which shows the u-quark and gluon PDFs. For the quark distribution, the high-Q^2 distributions SaS 2D and 2M are larger than the low-Q^2 ones 1D and 1M, simply reflecting the corresponding hierarchy in F_2^γ. At small x the opposite behaviour holds true since the small-x rise increases with the length of the Q^2 evolution. Hence the low-Q^2 parametrizations also yield larger gluon distributions at small x.

The effect of a non-zero target virtuality is displayed in Fig. 4. Increasing P^2 not only lowers the normalization but also changes the shape of the distribution. As expected, the gluon distribution vanishes faster than the quark distribution as $P^2 \to Q^2$.

4.5 The TPC/2γ parametrization and comparison with FKP

Experiments often use the TPC/2γ parametrization [19] of $F_2^\gamma(x, Q_0^2)$ determined at $Q_0^2 = 0.71\,\mathrm{GeV}^2$ to estimate the hadronic component of $F_2^\gamma(x, Q^2)$

$$\frac{1}{\alpha_{\rm em}} F_2^{\gamma,\rm VMD}(x, Q^2) \approx \frac{1}{\alpha_{\rm em}} F_2^\gamma(x, Q_0^2)|_{\rm TPC/2\gamma} \tag{52}$$

	a	b	c	d	e	f	g	κ
$c_1^{\rm val}$	1.168	1.771	29.35	–	–	–	–	5.776
$c_2^{\rm val}$	0.5	0.208	–	–	−0.794	1.516	–	–
$c_3^{\rm val}$	2.6	7.6	–	–	5.0	–	–	–
$c_4^{\rm val}$	–	5.15	–	–	2.0	–	–	–
$c_5^{\rm val}$	0.965	22.35	–	–	18.4	–	–	–
$c_6^{\rm val}$	1.0	–	–	–	–	–	–	–
$c_7^{\rm val}$	–	2.667	–	–	–	–	–	–
$c_1^{\rm sea}$	0.209	–	0.644	–	0.319	17.6	–	–
$c_2^{\rm sea}$	−0.373	−7.71	–	–	0.815	11.0	–	–
$c_3^{\rm sea}$	4.0	1.0	–	–	–	–	–	–
$c_4^{\rm sea}$	–	0.45	–	–	–	–	–	–
$c_1^{\rm g}$	1.808	29.9	–	–	26.4	–	–	5.28
$c_2^{\rm g}$	–	−5.35	−10.11	–	31.71	–	–	–
$c_3^{\rm g}$	2.0	−7.3	4.0	–	2.5	–	–	–
$c_4^{\rm g}$	–	10.9	–	–	2.5	–	–	–

Table 7: Coefficients of the hadronic distributions evolved from (51), parametrized in the form (49), where $c_i = \exp(-\kappa s)(a + bs + cs^2 + ds^3)/(1 + es + fs^2 + gs^3)$.

$$\equiv (0.22 \pm 0.01)\, x^{0.31\pm0.02}\,(1-x)^{0.95} + (0.06 \pm 0.01)\,(1-x)^{2.5\pm1.1}\ .$$

The full $F_2^\gamma(x, Q^2)$ distribution is then obtained by adding the FKP parametrization [20] of the anomalous part of F_2^γ to eq. (52). The only free parameter[2] in this aproach is the cutoff scale p_{T0} separating the perturbative part of F_2^γ from the non-perturbative one. Moreover, p_{T0} is often varied in the figures of $F_2^\gamma(x, Q^2)$ or $\int_{0.3}^{0.8} dx F_2^\gamma(x, Q^2)$ to illustrate the strong dependence on this arbitrary scale, implying little or no sensitivity of the data to the QCD scale Λ. This approach to compose F_2^γ from a hadronic and a perturbative part can be criticized on three counts:

1. The hadronic part of F_2^γ, eq. (52), is not evolved in Q^2.
2. The strong correlation between the scale p_{T0} and the size and shape of the hadronic part is neglected.
3. The FKP formula is a poor parametrization of the anomalous part.

Let us discuss these points in more detail.

The first point is obvious. In order to investigate how well the F_2^γ data can be described with eq. (52), one has to consider this equation as the non-perturbative input to $F_2^\gamma(x, Q^2)$ at the scale $Q_0^2 = 0.71\,\mathrm{GeV}^2$, whereafter it evolves with Q^2. Note that, for the Q^2 evolution, the input distributions have to be known separately for the valence, sea, and gluon distributions. It is sensible to assume that these hadronic input distributions can be interpreted within generalized vector-meson dominance (GVMD), in which case we can exploit eq. (41). Associating the first term of eq. (52) with valence quarks, we need a K-factor of $K = 1.411$ compared to simple VMD, eq. (39). This represents the contribution of additional vector mesons that have to be included in eqs. (11) and (39) because of the larger continuum cutoff $Q_0 = 0.84\,\mathrm{GeV}$ compared to the $\sim 0.6\,\mathrm{GeV}$ preferred for simple VMD.

[2]The values of the light-quark masses are needed as well, but these are supposed to be known.

The only free parameters are then Λ, a_g, and b_g. The fit to the F_2^γ data in the DIS scheme yields $\Lambda = 0.116\,\mathrm{GeV}$ and

$$\begin{aligned} Kx\ v(x) &= 0.57x^{0.31}(1-x)^{0.95} \\ Kx\ s(x) &= 0.082(1-x)^{2.5} \\ Kx\ g(x) &= 2.586x^{0.31}(1-x)^{0.95}\ . \end{aligned} \tag{53}$$

The photon momentum is approximately split as $3:1:6$ between valence quarks, sea quarks, and gluons at the input scale. In Fig. 5 we show the hadronic part of F_2^γ at $Q^2 = 4$ and $100\,\mathrm{GeV}^2$ as well as at the input scale $0.71\,\mathrm{GeV}^2$. The effect of the Q^2 evolution is non-negligible: a clearly visible softening at large x and an increase at small x is observed. The fit is, however, a rather bad representation of the data, in particular at high Q^2. This is reflected in a high χ^2 value, $\chi^2 = 181$. We therefore do not provide a parametrization for the distributions Q^2-evolved from eq. (52).

Concerning the second point, we recall that, by definition, the perturbative part of $F_2^\gamma(x,Q^2)$ vanishes at the Q_0 (or p_{T0}) scale separating it from the non-perturbative part of F_2^γ. Hence, any change in this scale has to be accompanied by a corresponding change in the size and shape of the hadronic input distributions at this scale. The correlation is obvious: the larger the Q_0, the smaller is the range of perturbative evolution, and hence the bigger is the non-perturbative input needed. If higher-twist effects can be neglected, the total photon momentum carried by partons should be independent of Q_0. Then eqs. (4) and (12) yield the following dependence on Q_0 for the normalization $K = K(Q_0)$ defined in eq. (36):

$$\begin{aligned} K(Q_0') &= K(Q_0) + \frac{\sum_\mathrm{q} e_\mathrm{q}^2}{\pi \sum_{V=\rho,\omega,\phi} 4\pi/f_V^2} \ln\frac{Q_0'^2}{Q_0^2} \\ &\approx K(Q_0) + 0.770 \ln\frac{Q_0'}{Q_0}\ . \end{aligned} \tag{54}$$

Also a correlation between the separation scale and the x-shape is to be expected, with harder hadronic input distributions required for larger Q_0 scales. This could be argued on the basis of GVMD, or simply by the fact that parts of the (hard) perturbative $\gamma \to \mathrm{q\overline{q}}$ splittings have to be included in the "hadronic" input distributions for larger Q_0. In any case, the separation scale is an arbitrary parameter and hence the result for F_2^γ *must not depend* on its value, provided it is changed within a range in which leading-twist perturbative QCD describes the physics. As the comparison of our various parametrizations demonstrates, even the variation of the scale between 0.6 GeV and 2.0 GeV has not a major influence on the final F_2^γ result. (The differences that are there come from them being fits to different data sets, i.e. data with $Q < 2$ GeV included or not. One can do a $Q_0 = 0.6$ GeV fit to $Q > 2$ GeV data only, and then obtain close agreement with a $Q_0 = 2$ GeV fit.)

As to point 3 above, a solution of the perturbatively calculable part of the quark distribution functions of the photon has been obtained by FKP [20]:

$$f_\mathrm{q}^{\gamma,\mathrm{anom}}(x,Q^2) = \frac{\alpha_\mathrm{em}}{2\pi}\, 3\, e_\mathrm{q}^2\, \frac{x^2+(1-x)^2}{x^C + Cf(x)}\, \Upsilon \left[1 - \left(\frac{\Upsilon_0}{\Upsilon}\right)^{1+Cf(x)}\right]\ , \tag{55}$$

where

$$C = \frac{8}{33-2N_f} \qquad f(x) = 2\ln\frac{1}{1-x} - x - \frac{1}{2}x^2$$

$$\Upsilon = \ln \frac{t_{\max}}{\Lambda^2} \qquad t_{\max} = \frac{Q^2}{x}$$
$$\Upsilon_0 = \ln \frac{t_0}{\Lambda^2} \qquad t_0 = \frac{m_{T0}^2}{1-x} \equiv \frac{m_{\rm q}^2 + p_{T0}^2 + x(1-x)P^2}{1-x} \; . \tag{56}$$

Here t_0 is the cutoff in the integration over the virtuality of the t-channel and u-channel quark propagators and P^2 the target mass (virtuality of the probed photon). In Fig. 6a we compare our anomalous u-quark distribution function at $Q^2 = 4\,\mathrm{GeV}^2$, $P^2 = 0$, and $Q_0^2 = 0.36\,\mathrm{GeV}^2$ with eq. (55), where we have taken the FKP value for the quark mass ($m_{\rm q} = 0.3\,\mathrm{GeV}$) but adjusted p_{T0} such that $m_{T0}^2 = Q_0^2$.

It might seem surprising that the two distributions do not at all agree with each other. The difference arises mainly from the inclusion of the $1/x$ and $1/(1-x)$ factors in eq. (56) ($1/x$ in $t_{\max}$ and Υ, $1/(1-x)$ in t_0 and Υ_0). These terms are of kinematic origin and specific to the quark-parton-model result (calculation of the box diagram). However, their inclusion in the leading-twist QCD evolution equations lacks justification in perturbative QCD: the leading-logarithmic approximation sums only the logarithms in Q^2/Λ^2 and makes no statement about the summation of $\ln x$ or $\ln(1-x)$ terms (beyond, of course, the double-leading-logarithmic approximation). In other words: although the factorization scale is arbitrary and may well differ from its "natural" value Q^2, it must not depend on x in order not to spoil factorization.

On the other hand, it is satisfying to observe that the FKP parametrization agrees almost perfectly with ours at large x if we take $t_{\max} = Q^2$ and $t_0 = m_{T0}^2$ in eq. (56). Differences at small x arise because eq. (55) was derived in the valence approximation, hence $xf_{\rm q}$ given in eq. (55) vanishes as $x \to 0$ while the full solution gives $xf_{\rm q}$ rising at small x.

Of course, one could argue that the FKP formula is not meant as a parametrization of quark distributions but as part of an $F_2^\gamma(x,Q^2)$ parametrization, in combination with VMD and direct terms. (After all, it is the FKP F_2^γ expression that is being used in the experimental analyses.) In this context, $\ln x$ and $\ln(1-x)$ terms may well be redistributed from the direct term into the "quark distribution" if this provides a convenient approximation to the full solution. The FKP prescription for F_2^γ is

$$F_2^{\gamma,\mathrm{anom}}(x,Q^2) = 2\sum_{\rm q} e_{\rm q}^2\, x \; \left\{ f_{\rm q}^{\gamma,\mathrm{anom}}(x,Q^2) \right.$$
$$\left. + \frac{\alpha_{\rm em}}{2\pi}\, 3\, e_{\rm q}^2 \left[6x(1-x) - 1 + \frac{2xm_{\rm q}^2 - x(1-x)P^2}{m_{T0}^2} \right] \right\} \; . \tag{57}$$

Figure 6b compares the u-quark component of eq. (57) with our parametrization of the anomalous u-quark distribution function, to which we add the u-quark component of the universal direct term eq. (45), i.e.

$$C_{\rm u}^\gamma(x) = \frac{\alpha_{\rm em}}{2\pi}\, 3 \left(\frac{2}{3}\right)^2 x \; \left\{ \left[x^2 + (1-x)^2\right] \ln\frac{1}{x} + 6x(1-x) - 1 \right\} \; . \tag{58}$$

The observable discrepancy is, in fact, not unexpected as no $\ln(1-x)$ term is included in eq. (58). However, a discrepancy remains even when the $\ln(1-x)$ factor is removed from the definition of Υ_0 in the FKP formula.

The reason for this is the extra $m_{\rm q}^2/m_{T0}^2$ term in eq. (57). Indeed, when we take $m_{\rm q} = 0$ and $t_0 = Q_0^2$ in eqs. (56) and (57), we find agreement at large x between our anomalous-plus-direct u-quark distribution function and the FKP one, Fig. 6c. Alternatively we

also expect agreement for the comparison of the standard FKP result, i.e. where $t_0 = Q_0^2/(1-x)$, if we change from the expression (58) for the direct term to the standard direct term, eq. (43):

$$C_{\rm u}^{\gamma}(x) = \frac{\alpha_{\rm em}}{2\pi}\, 3\, \left(\frac{2}{3}\right)^2 x\, \left\{ \left[x^2 + (1-x)^2\right] \ln\frac{1-x}{x} + 8x(1-x) - 1 \right\}\,, \qquad (59)$$

which includes the $\ln(1-x)$ term. This is, however, not the case. The difference can be traced back to the difference in the coefficient of the $x(1-x)$ term in eq. (57) and in eq. (59). Indeed, we obtain agreement with the standard FKP result at large x if we add to our parametrization of the u-quark distribution function the following direct term:

$$C_{\rm u}^{\gamma}(x) = \frac{\alpha_{\rm em}}{2\pi}\, 3\, \left(\frac{2}{3}\right)^2 x\, \left\{ \left[x^2 + (1-x)^2\right] \ln\frac{1-x}{x} + 6x(1-x) - 1 \right\}\,. \qquad (60)$$

In conclusion, putting $m_{\rm q}$ equal to zero and changing the $6x(1-x)$ term into $8x(1-x)$ in eq. (57), the FKP parametrization describes rather well the leading-twist, leading-order anomalous part of $F_2(x,Q^2)$ at large x in the (standard) DIS scheme. However, a number of problems remain:

- The unmodified FKP expression (57) includes extra terms that have no correspondence in perturbative QCD: they are neither leading-twist NLO terms nor higher-twist contributions. These terms depend on an additional, unphysical parameter, the light-quark masses.
- The FKP result is obtained in the valence approximation, and thus does not reproduce the correct small-x behaviour of F_2 (which, actually, matters already for $x < 0.5$).
- A hadronic part of F_2^{γ} matched to the FKP parametrization is not available. The recipe "TPC/2γ-plus-FKP" is inconsistent: since the FKP parametrization needs a $p_{T0} \leq 0.5\,\text{GeV}$ to describe the high-Q^2 data, FKP is already large at $Q^2 = 0.71\,\text{GeV}^2$, where the TPC parametrization alone is supposed to describe the data.
- Since the FKP parametrization in eq. (55) mixes kinematic terms between the evolved quark distribution functions and the direct term, it is not a parametrization of the anomalous quark distribution functions of the photon (at least not with default parameters). The quark distribution functions do not show the correct small-x behaviour and a parametrization of the gluon density is missing.

We have attempted to provide an alternative where these problems are resolved. Our quark and gluon distribution functions obey the leading-logarithmic evolution equations down to very small x ($\sim 10^{-4}$). The only free parameter besides Λ is the scale Q_0. Moreover, for two representative values of Q_0 (0.6 and 2.0 GeV), our anomalous PDFs are supplemented by parametrizations of the hadronic PDFs. These have been obtained by fitting the photon structure function $F_2^{\gamma}(x,Q^2)$ to the available data.

5 Concluding remarks

In this paper we have shown how the PDFs of the photon can be decomposed into perturbative and non-perturbative components. Since this separation and the constraints on the non-perturbative part is the central result of our paper, we briefly repeat the main ideas of our approach and show its connection with an integral representation of the photon structure functions. Our starting point is the fact that a PDF, being the solution of an

inhomogeneous evolution equation, can always be written as the sum of two terms: a particular solution $f_a^{\gamma,\mathrm{PT}}(x,Q^2,Q_0^2)$, which vanishes at $Q^2=Q_0^2$, and a general solution $f_a^{\gamma,\mathrm{NP}}(x,Q^2,Q_0^2)$ of the corresponding homogeneous evolution equation, that needs an input at $Q^2=Q_0^2$. For Q_0 sufficiently large, such that higher-twist $(1/Q^2)$ effects become negligible, the anomalous distribution function defined in eq. (8) is a particular solution. Hence we can identify $f_a^{\gamma,\mathrm{PT}}(x,Q^2,Q_0^2)=f_a^{\gamma,\mathrm{anom}}(x,Q^2,Q_0^2)$.

To constrain $f_a^{\gamma,\mathrm{NP}}(x,Q^2,Q_0^2)$ we first observe that the anomalous distribution function of a parton a within the photon is the convolution of two factors. The first one, $P^\gamma_{\mathrm{q\overline{q}}}(k)=(\alpha_{\mathrm{em}}/2\pi)2e_{\mathrm{q}}^2\mathrm{d}k^2/k^2$ gives the probability for the photon to branch into a $\mathrm{q\overline{q}}$ state at some (perturbatively high) scale k. The second factor is the distribution function of the parton a within this $\mathrm{q\overline{q}}$ state. This "state" distribution function obeys the homogeneous evolution equation (with the calculable input (9)).

This factorization of $f_a^{\gamma,\mathrm{PT}}$ suggests a similar one for $f_a^{\gamma,\mathrm{NP}}(x,Q^2,Q_0^2)$. Below the scale Q_0, the $\gamma\to\mathrm{q\overline{q}}$ transition can no longer be calculated perturbatively but may be approximated by fluctuations of the photon into vector mesons with probabilities $P_V^\gamma(k^2=m_V^2)=4\pi\alpha_{\mathrm{em}}/f_V^2$. Hence the analogue of the k-integral above Q_0 of the continuous spectrum of perturbative ("anomalous") states is the discrete sum of vector mesons, with the state distribution functions $f_a^{\gamma,\mathrm{q\overline{q}}}$ replaced by the PDFs $f_a^{\gamma,V}$ of the $\mathrm{q\overline{q}}$ "bound states" V of the photon. As long as the shape of these distribution functions are treated as free parameters (to be fixed from data), $f_a^{\gamma,\mathrm{NP}}=f_a^{\gamma,\mathrm{VMD}}$ defined in eq. (11) is indeed a general solution of the homogeneous evolution equations.

Our decomposition (34) also follows from the representation of the (moments of the) photonic PDFs as a dispersion integral in the photon mass (P^2 is the photon virtuality) [27]

$$f_a^\gamma(n,Q^2,P^2)=\int_0^{Q^2}\frac{\mathrm{d}k^2}{k^2+P^2}\rho_a(n,Q^2,k^2)\;. \tag{61}$$

Rather than describing the dispersion integral as the difference between a "point-like" part (contribution from the upper limit) and a "hadronic" part (contribution from the lower limit), it is more natural to separate short-distance and long-distance parts by a scale Q_0 since the weight function ρ_a possesses the scaling-violation pattern typical of ordinary hadronic PDFs [27]. Our solution follows from the ansatz

$$\begin{aligned}\rho_a(n,Q^2,k^2)=&\frac{\alpha_{\mathrm{em}}}{\pi}e_{\mathrm{q}}^2f_a^{\gamma,\mathrm{q\overline{q}}}(n,Q^2,k^2)\Theta(k^2-Q_0^2)\\&+\sum_V\frac{4\pi\alpha_{\mathrm{em}}}{f_V^2}\delta'\left(1-\frac{k^2}{m_V^2}\right)f_a^{\gamma,V}(n,Q^2,Q_0^2)\;.\end{aligned} \tag{62}$$

The scale Q_0 is arbitrary; hence the Q_0 dependence of the anomalous part must be cancelled by that of the hadronic one. For example, in the generalized vector-meson-dominance ansatz (36) that we are using, the relation between the two parts is given by eq. (54).

For a given, chosen Q_0, the only unknown (non-perturbative) pieces of the photon structure functions and the PDFs of the photon are the valence, sea, and gluon input distributions and the value of K in eq. (36). In order to cover the uncertainties associated with our approach we have presented two extreme analyses. In the first we restricted VMD to the well-established ρ^0, ω, ϕ states only (i.e. $K=1$) and fixed $Q_0=0.6\,\mathrm{GeV}$ as obtained from our γp analysis. Here the main theoretical error arises from the use of perturbation theory down to rather low values of Q^2. The spirit of the second analysis was opposite: take Q_0 well within the perturbative domain ($Q_0=2\,\mathrm{GeV}$) at the expense

of parametrizing the effects of additional vector mesons by a simple factor K to be fitted to the data.

We have presented self-contained formulae and parametrizations that allow the PDFs and F_2 of the photon to be evaluated as a function of x and Q^2, and also for non-vanishing target virtuality P^2. A program with this information already encoded is obtainable on request from the authors. The anomalous PDFs are parameter-free; more precisely, the parametrization depends analytically on Q_0, Λ, and P^2 (besides, of course , Q^2 and x). Similarly, the state distributions can be evaluated for arbitray x, Q^2, k^2, and Λ. Based on fits to the available $F_2^\gamma(x, Q^2)$ data, four different sets of hadronic PDFs are provided in order to illustrate the uncertainties in current PDF determinations. The sets differ in the value of Q_0 (0.6 and 2 GeV) and the data included (in both cases only data above Q_0^2 are included in the fit), and the factorization scheme. The latter dependence is formally of NLO accuracy, but is found to be numerically significant in LO analyses.

We have outlined the small-x behaviour of the PDFs and also discussed the description of the hadronic event properties in photon-induced reactions. A proper treatment requires knowledge beyond that of the usual inclusive PDF parametrizations. Moreover, we have investigated how the photon-to-$\mathrm{q\overline{q}}$ splitting probability enters the eikonalization of jet cross sections. We have derived a formula that ensures that the various contributions are not counted twice. We have shown that it is mandatory to change from the inclusive PDFs to the state distributions.

Finally we have investigated the limitations of the approximation of $F_2^\gamma(x, Q^2)$ by the "FKP-plus-TPC/2γ" expression. We found that (with correct parameter choice) the FKP formula is a good parametrization of the anomalous part of $F_2^\gamma(x, Q^2)$ at large x but fails for $x < 0.5$. Concerning the parametrization of the hadronic part, we demonstrated the effects of the necessary Q^2 evolution of the TPC/2γ parametrization and, most importantly, pointed out the strong correlation between the cutoff scale p_{T0} of the FKP formula and the (size and shape of the) hadronic part: if p_{T0} is varied only in the anomalous part, it introduces an artificial dependence on an unphysical parameter, which must not be there.

Acknowledgement

We thank A. Vogt for providing us with tables of F_2^γ data.

References

[1] C. Berger and W. Wagner, Phys. Rep. **146** (1987) 1

[2] H. Kolanoski and P. Zerwas, in *High-energy electron–positron physics* (World Scientific, Singapore, 1988), eds. A. Ali and P. Söding, p. 695

[3] J.H. Da Luz Vieira and J.K. Storrow, Z. Phys. **C51** (1991) 241

[4] F.M. Borzumati and G.A. Schuler, Z. Phys. **C58** (1993) 139

[5] A. Vogt, in *Proc. of the Workshop on Two-Photon Physics at LEP and HERA* (Lund, Sweden, 1994), eds. G. Jarlskog and L. Jönsson, p. 141

[6] S.J. Brodsky and P.M. Zerwas, SLAC-PUB-6571, July 1994; to appear in *Proc. of the Workshop on $\gamma\gamma$ Colliders*, LBL, USA, March 1994

[7] D.J. Miller, in *Proc. of the Workshop on Two-Photon Physics at LEP and HERA* (Lund, Sweden, 1994), eds. G. Jarlskog and L. Jönsson, p. 4

[8] M. Drees and K. Grassie, Z. Phys. **C28** (1985) 451;
H. Abramowicz, K. Charchula and A. Levy, Phys. Lett. **B269** (1991) 458;
K. Hagiwara, M. Tanaka, I. Watanabe and T. Izubuchi, "Gluon and charm distributions in the photon", KEK preprint 93-160, March 1994 (hep-ph 9406252)

[9] M. Glück, E. Reya and A. Vogt, Phys. Rev. **D46** (1992) 1973

[10] P. Aurenche, M. Fontannaz and J.-Ph. Guillet, LAPP preprint ENSLAPP-A-435-93-REV, 1993

[11] L.E. Gordon and J.K. Storrow, Z. Phys. **C56** (1992) 307

[12] G.A. Schuler and T. Sjöstrand, Phys. Lett. **B300** (1993) 169 and Nucl. Phys. **B407** (1993) 539

[13] T.F. Walsh and P.M. Zerwas, Nucl. Phys. **B41** (1972) 551 and Phys. Lett. **B44** (1973) 195;
R. Kingsley, Nucl. Phys. **B60** (1973) 45 4

[14] T. Uematsu and T.F. Walsh, Phys. Lett. **B101** (1981) 263 and Nucl. Phys. **B199** (1982) 93;
G. Rossi, Univ. California at San Diego preprint UCSD-10P10-227 (1983) and Phys. Rev. **D29** (1984) 852

[15] S.M. Kim and T.F. Walsh, Univ. of Minnesota preprint UMN-TH-1111-92, September 1992, hep-ph-9308267

[16] M. Drees and R.M. Godbole, Madison preprint MAD/PH/819, March 1994

[17] P. Aurenche, J.-Ph. Guillet, M. Fontannaz, Y. Shimizu, J. Fujimoto and K. Kato, in *Proc. of the Workshop on Two-Photon Physics at LEP and HERA* (Lund, Sweden, 1994), eds. G. Jarlskog and L. Jönsson, p. 267

[18] M. Glück, E. Reya and M. Stratmann, Dortmund preprint DO-TH 94/14, August 1994

[19] TPC/2γ collab., H. Aihara et al., Z. Phys. **C34** (1987) 1 and Phys. Rev. Lett. **58** (1997) 97

[20] J.H. Field, F. Kapusta and L. Poggioli, Phys. Lett. **B181** (1986) 362 and Z. Phys. **C36** (1987) 121;
F. Kapusta, Z. Phys. **C42** (1989) 225

[21] C. Peterson, T.F. Walsh and P.M. Zerwas, Nucl. Phys. **B229** (1983) 301

[22] R. Odorico, Phys. Lett. **B102** (1981) 341 and Comput. Phys. Commun. **25** (1982) 253

[23] F. James, "MINUIT — Function Minimization and Error Analysis", version 92.1 (March 1992), CERN Program Library D506, CERN, Geneva 1992

[24] Yu.L. Dokshitzer and D.V. Shirkov, LU TP 93-19

[25] V.M. Budnev et al., Phys. Rep. **15** (1975) 181

[26] C.T. Hill and G.G. Ross, Nucl. Phys. **B148** (1979) 373

[27] J.D. Bjorken, "Two topics in quantum chromodynamics", SLAC-PUB-5103, December 1989

[28] JADE collab., W. Bartel et al., Z. Phys. **C24** (1984) 231

[29] PLUTO collab., Ch. Berger et al., Z. Phys. **C26** (1984) 353 and Nucl. Phys. **B281** (1987) 365

[30] TASSO collab., H. Althoff et al., Z. Phys. **C31** (1986) 527

[31] AMY collab., T. Sasaki et al., Phys. Lett. **252** (1990) 491

[32] CELLO collab., H.J. Behrend et al., contributed paper to the XXVth Int. Conf. on HEP, Singapore, 1990

[33] TOPAZ collab., K. Muramatsu et al., Phys. Lett. **B332** (1994) 477

[34] OPAL collab., R. Akers et al., Z. Phys. **C61** (1994) 199

Figure 1: Comparison of the fits with the available [28, 29, 30, 19, 31, 32, 33, 34] F_2^γ data. The full curve is for set SaS 1D, dashed for SaS 1M, dash-dotted SaS 2D and dotted SaS 2M. Data at nearby Q^2 values are shown in the same frame, and the theoretical curves are evaluated at some average Q^2 value of that range. The small vertical bars through the curves indicate the x value where $W = 1$ GeV. The behaviour to the right of this point should be taken as indicative only, with the possibility of large higher-twist contributions.

Figure 2: Subdivision of the full F_2^γ parametrization by component, compared with data at $Q^2 \approx 5.2$ GeV^2. The total F_2^γ is shown by the full curve. The lowest dashed curve gives the VMD contribution, and the next lowest the sum of VMD and anomalous ones. The third dashed curve, which coincides with the full curve for the DIS fits, gives the sum of VMD, anomalous and Beithe–Heitler terms. For the $\overline{\rm MS}$ fits, the full curve additionally contains the contribution of the C^γ term. Note that this last term is negative at large x.

Figure 3: Comparison of parametrizations of the u-quark and gluon PDFs at $Q^2 = 4, 40$ and 400 GeV^2. Full curve is for set SaS 1D, dashed for SaS 1M, dash-dotted SaS 2D and dotted SaS 2M, as in Fig. 1. Note that a logarithmic y scale is used for the gluon distribution. For $Q^2 = 400$ GeV^2 also the x axis is logarithmic, so as better to show differences in the small-x behaviour.

Figure 4: Target-mass (P^2) dependence of the u-quark and gluon PDFs, for $Q^2 = 10\,\text{GeV}^2$. From top to bottom: $\sqrt{P^2} = 0$, 0.2 GeV, 0.7 GeV, and 1.4 GeV. The top two frames are for set SaS 1D, and the bottom two for set SaS 2M. The remaining two look similar qualitatively.

Figure 5: The hadronic part of $F_2^\gamma(x, Q^2)$ as obtained by evolving the TPC/2γ parametrization of F_2^γ. The full curve is the x dependence at the input scale $Q^2 = 0.71\,\text{GeV}^2$, dashed curve at $4\,\text{GeV}^2$, and dash-dotted curve at $100\,\text{GeV}^2$.

Figure 6: Comparison between the FKP and our parametrizations of the anomalous u-quark distribution as a function of x. The x and $xu(x)$ values are shown in linear scale to the left and in logarithmic scale to the right. Common values are $Q^2 = 4\,\text{GeV}^2$, $P^2 = 0$, $n_f = 3$, and $\Lambda_3 = 230\,\text{MeV}$; additionally $Q_0^2 = 0.36\,\text{GeV}^2$ in our parametrization.
a) The full curve is our parametrization, dashed curve is FKP with $t_{\max} = Q^2/x$ and $t_0 = Q_0^2/(1-x)$, and dotted curve is FKP with $t_{\max} = Q^2$ and $t_0 = Q_0^2$.
b) The full curve is our parametrization plus our direct term (58), dashed curve is FKP with their direct term (57), $m_{\rm q}/p_{T0} = 0.3/0.52$, $t_{\max} = Q^2/x$ and $t_0 = Q_0^2/(1-x)$, and dash-dotted curve is FKP as above except that $t_0 = Q_0^2$.
c) The full curve is our parametrization plus our direct term (58), large-dotted curve is our parametrization plus the standard direct term (59), dotted curve is our parametrization plus the modified direct term (60), dashed curve is FKP with their direct term (57), $m_{\rm q}/p_{T0} = 0./0.6$, $t_{\max} = Q^2/x$ and $t_0 = Q_0^2/(1-x)$, and dash-dotted curve is FKP as above, except that $t_0 = Q_0^2$.

This figure "fig1-1.png" is available in "png" format from:

http://arXiv.org/ps/hep-ph/9503384v1

This figure "fig1-2.png" is available in "png" format from:

http://arXiv.org/ps/hep-ph/9503384v1

This figure "fig1-3.png" is available in "png" format from:

http://arXiv.org/ps/hep-ph/9503384v1

This figure "fig1-4.png" is available in "png" format from:

http://arXiv.org/ps/hep-ph/9503384v1

This figure "fig1-5.png" is available in "png" format from:

http://arXiv.org/ps/hep-ph/9503384v1

This figure "fig1-6.png" is available in "png" format from:

http://arXiv.org/ps/hep-ph/9503384v1

This figure "fig1-7.png" is available in "png" format from:

http://arXiv.org/ps/hep-ph/9503384v1

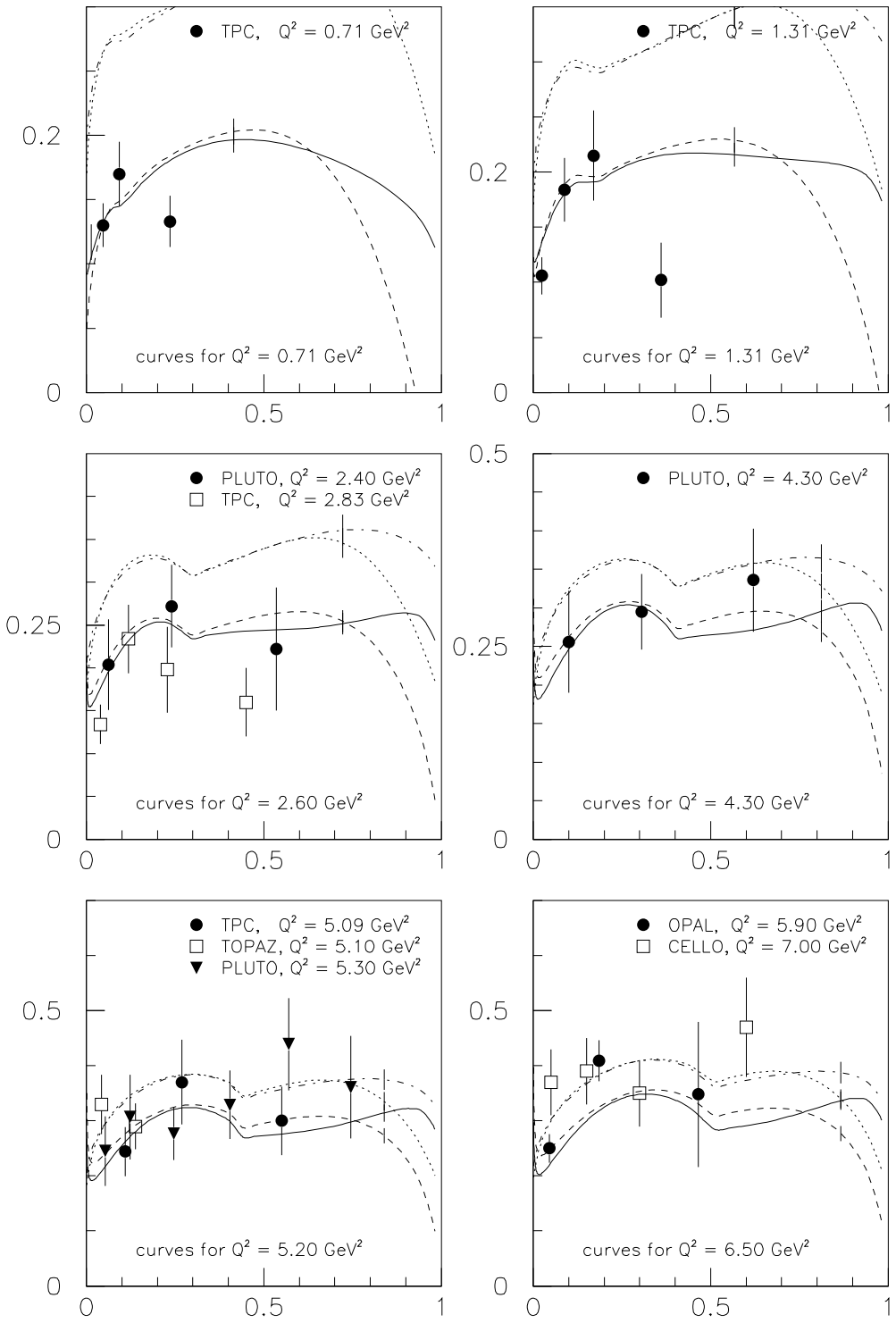

Figure 1: Comparison of the fits with the available [28, 29, 30, 19, 31, 32, 33, 34] F_2^γ data. The full curve is for set SaS 1D, dashed for SaS 1M, dash-dotted SaS 2D and dotted SaS 2M. Data at nearby Q^2 values are shown in the same frame, and the theoretical curves are evaluated at some average Q^2 value of that range. The small vertical bars through the curves indicate the x value where $W = 1$ GeV. The behaviour to the right of this point should be taken as indicative only, with the possibility of large higher-twist contributions.

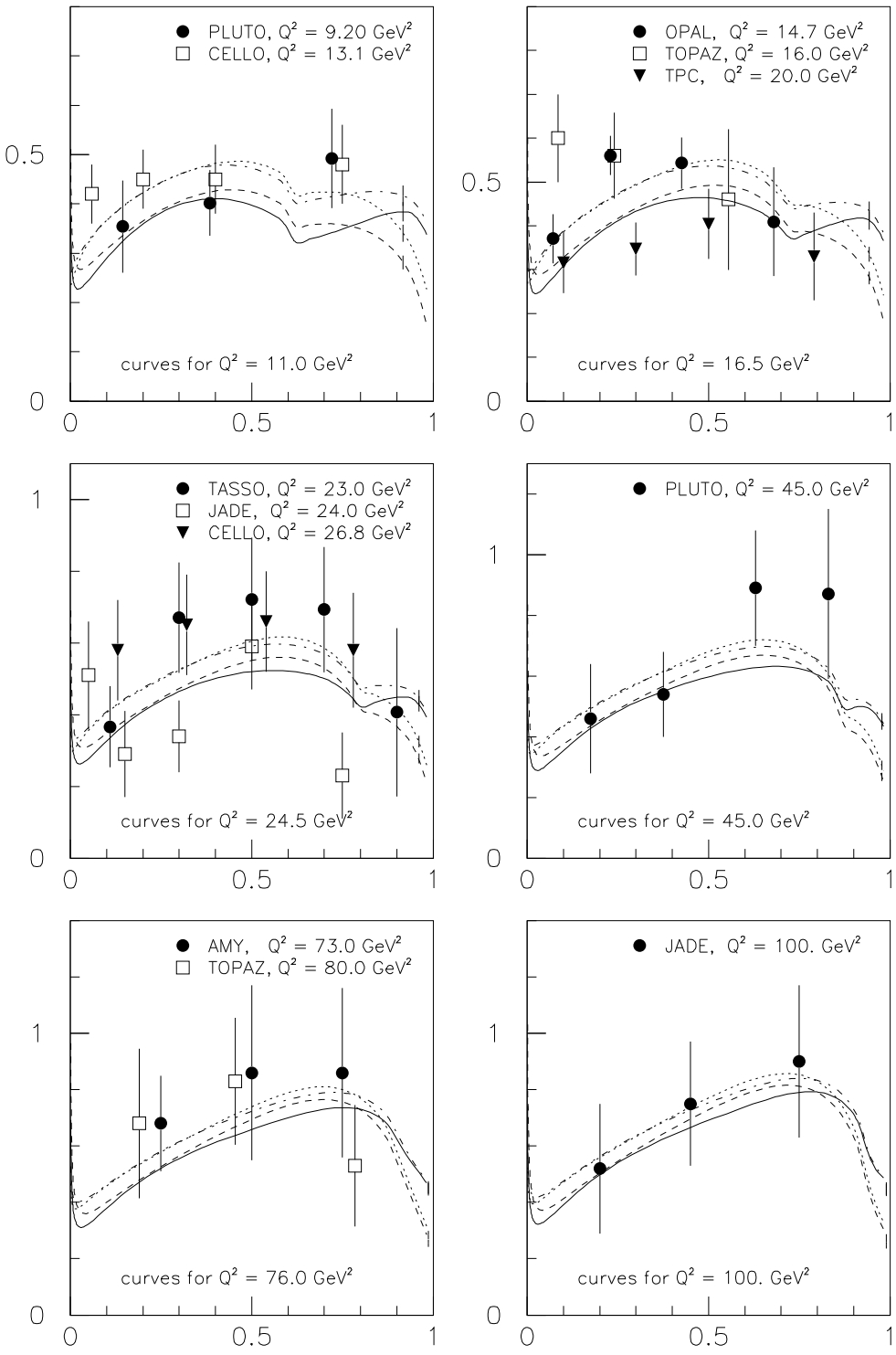

Figure 1: Continuation from previous page.

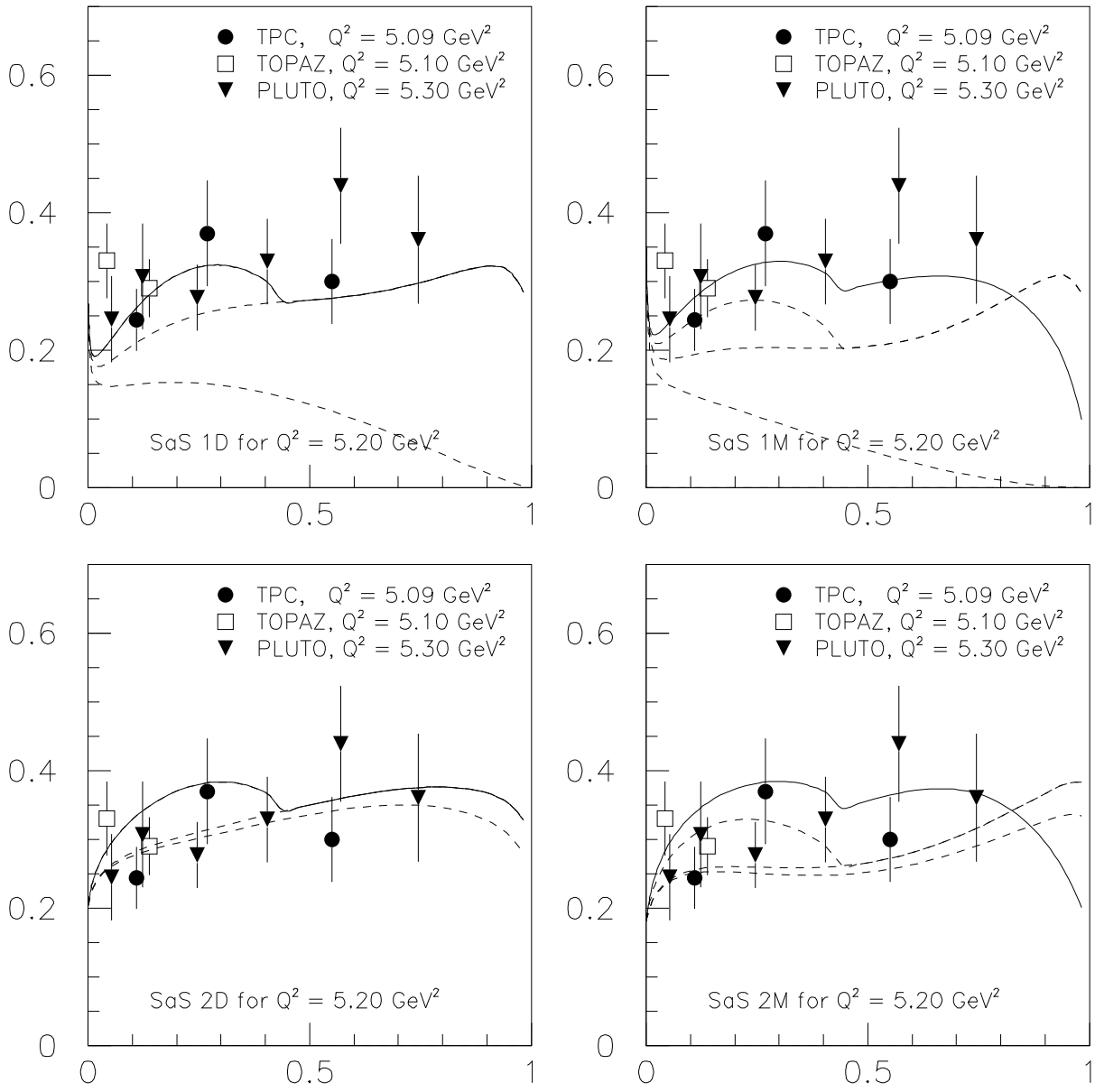

Figure 2: Subdivision of the full F_2^γ parametrization by component, compared with data at $Q^2 \approx 5.2$ GeV^2. The total F_2^γ is shown by the full curve. The lowest dashed curve gives the VMD contribution, and the next lowest the sum of VMD and anomalous ones. The third dashed curve, which coincides with the full curve for the DIS fits, gives the sum of VMD, anomalous and Beithe–Heitler terms. For the $\overline{\rm MS}$ fits, the full curve additionally contains the contribution of the C^γ term. Note that this last term is negative at large x.

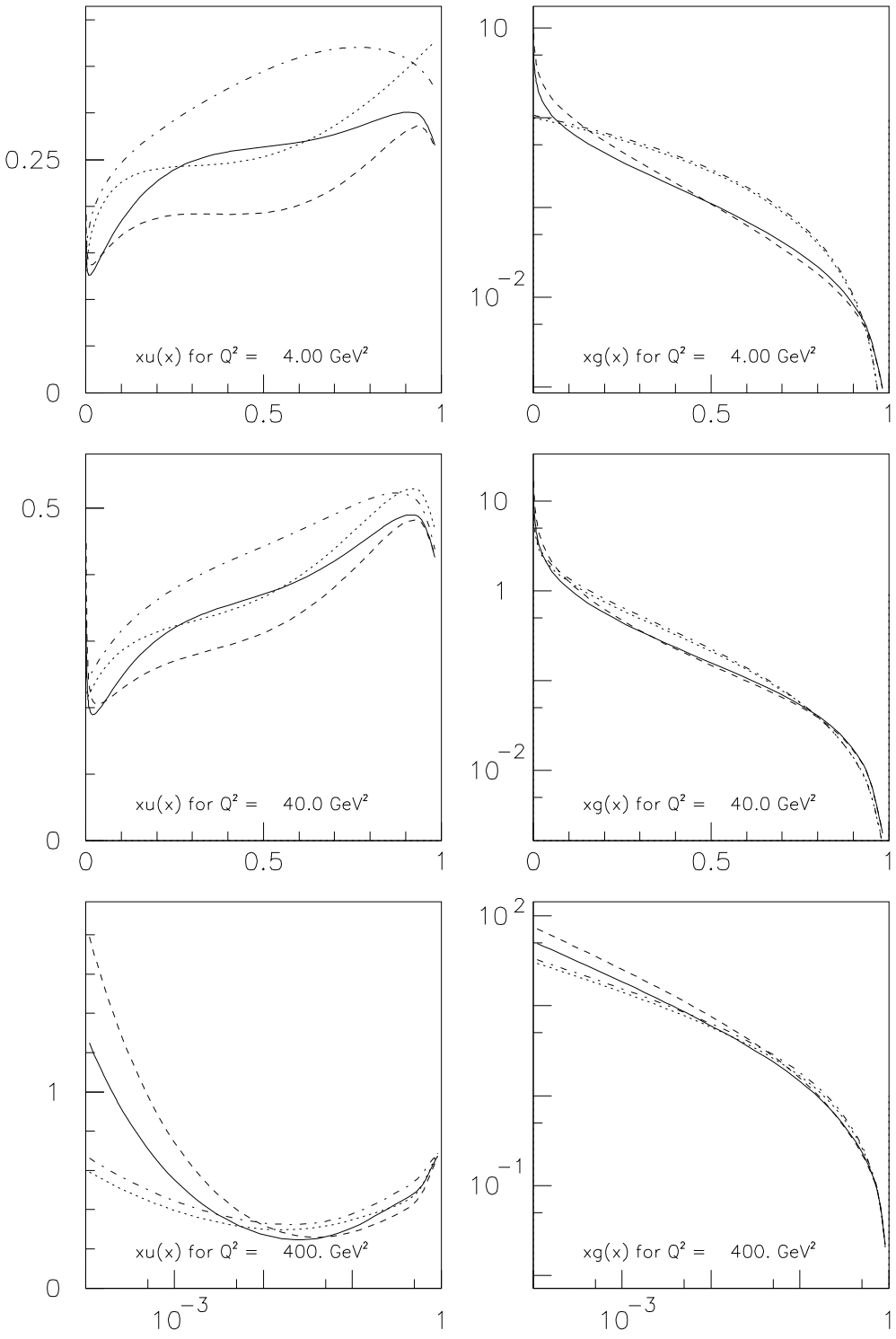

Figure 3: Comparison of parametrizations of the u-quark and gluon PDFs at $Q^2 = 4, 40$ and 400 GeV^2. Full curve is for set SaS 1D, dashed for SaS 1M, dash-dotted SaS 2D and dotted SaS 2M, as in Fig. 1. Note that a logarithmic y scale is used for the gluon distribution. For $Q^2 = 400$ GeV^2 also the x axis is logarithmic, so as better to show differences in the small-x behaviour.

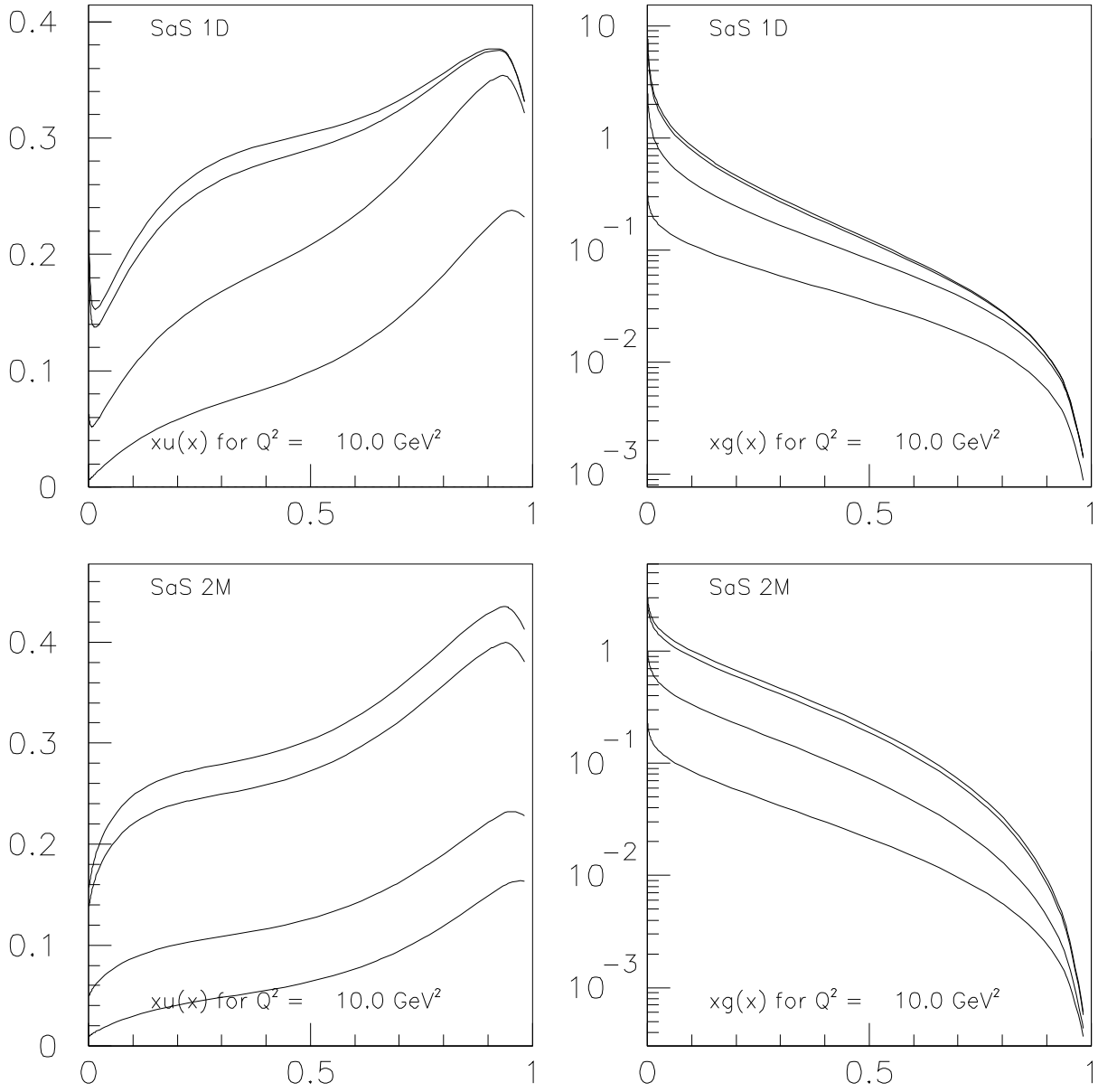

Figure 4: Target-mass (P^2) dependence of the u-quark and gluon PDFs, for $Q^2 = 10$ GeV^2. From top to bottom: $\sqrt{P^2} = 0$, 0.2 GeV, 0.7 GeV, and 1.4 GeV. The top two frames are for set SaS 1D, and the bottom two for set SaS 2M. The remaining two look similar qualitatively.

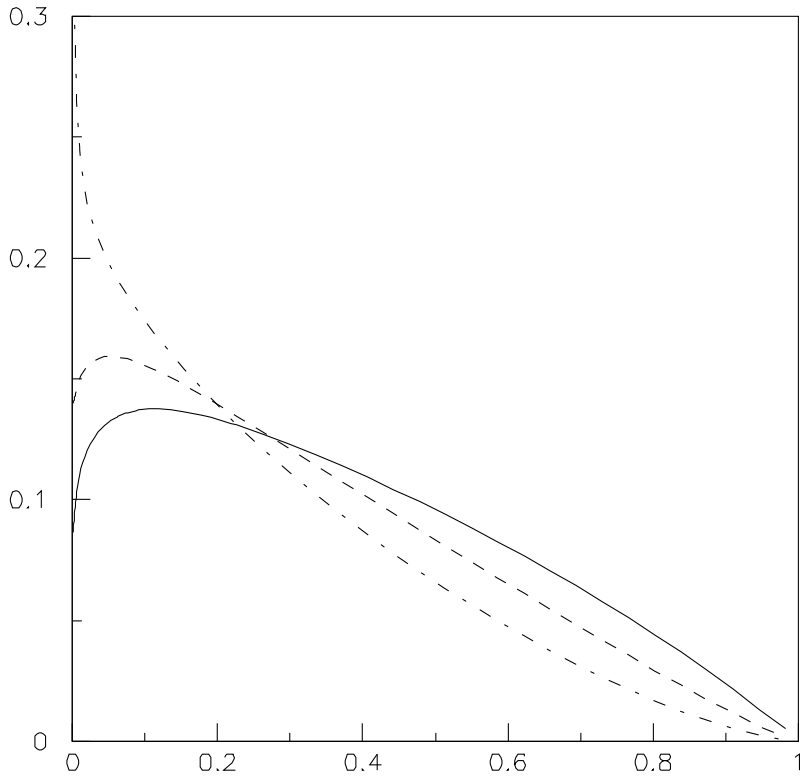

Figure 5: The hadronic part of $F_2^\gamma(x,Q^2)$ as obtained by evolving the TPC/2γ parametrization of F_2^γ. The full curve is the x dependence at the input scale $Q^2 = 0.71\,\mathrm{GeV}^2$, dashed curve at $4\,\mathrm{GeV}^2$, and dash-dotted curve at $100\,\mathrm{GeV}^2$.

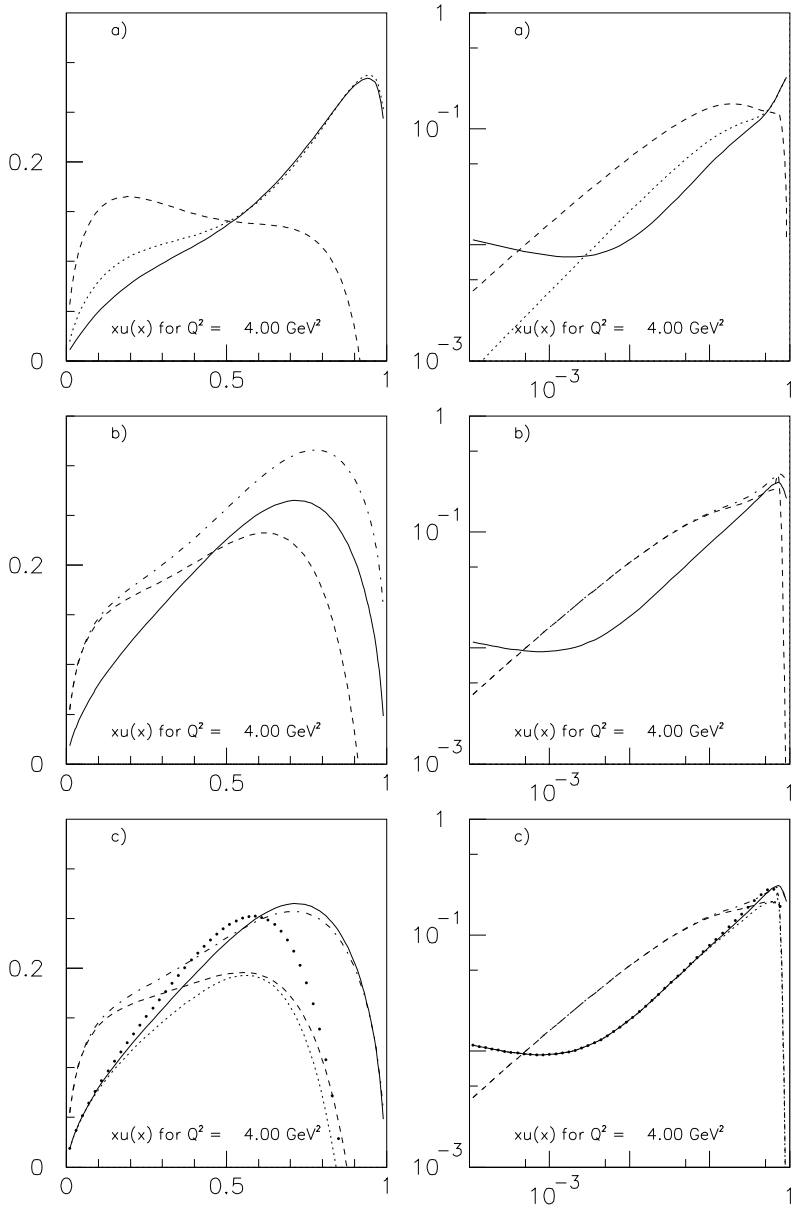

Figure 6: Comparison between the FKP and our parametrizations of the anomalous u-quark distribution as a function of x. The x and $xu(x)$ values are shown in linear scale to the left and in logarithmic scale to the right. Common values are $Q^2 = 4\,\mathrm{GeV}^2$, $P^2 = 0$, $n_f = 3$, and $\Lambda_3 = 230\,\mathrm{MeV}$; additionally $Q_0^2 = 0.36\,\mathrm{GeV}^2$ in our parametrization.
a) The full curve is our parametrization, dashed curve is FKP with $t_{\max} = Q^2/x$ and $t_0 = Q_0^2/(1-x)$, and dotted curve is FKP with $t_{\max} = Q^2$ and $t_0 = Q_0^2$.
b) The full curve is our parametrization plus our direct term (58), dashed curve is FKP with their direct term (57), $m_{\mathrm{q}}/p_{T0} = 0.3/0.52$, $t_{\max} = Q^2/x$ and $t_0 = Q_0^2/(1-x)$, and dash-dotted curve is FKP as above except that $t_0 = Q_0^2$.
c) The full curve is our parametrization plus our direct term (58), large-dotted curve is our parametrization plus the standard direct term (59), dotted curve is our parametrization plus the modified direct term (60), dashed curve is FKP with their direct term (57), $m_{\mathrm{q}}/p_{T0} = 0./0.6$, $t_{\max} = Q^2/x$ and $t_0 = Q_0^2/(1-x)$, and dash-dotted curve is FKP as above, except that $t_0 = Q_0^2$.